NASA TN D-1428

TECHNICAL NOTE

D-1428

A 1-FOOT HYPERVELOCITY SHOCK TUNNEL IN WHICH HIGH-ENTHALPY, REAL-GAS AIR FLOWS CAN BE GENERATED WITH FLOW TIMES OF ABOUT 180 MILLISECONDS

By Bernard E. Cunningham and Samuel Kraus

Ames Research Center
Moffett Field, Calif.

NATIONAL AERONAUTICS AND SPACE ADMINISTRATION

WASHINGTON

October 1962

NATIONAL AERONAUTICS AND SPACE ADMINISTRATION

TECHNICAL NOTE D-1428

A 1-FOOT HYPERVELOCITY SHOCK TUNNEL IN WHICH HIGH-ENTHALPY, REAL-GAS AIR FLOWS CAN BE GENERATED WITH FLOW TIMES OF ABOUT 180 MILLISECONDS

By Bernard E. Cunningham and Samuel Kraus

SUMMARY

A shock tunnel is described in which high-enthalpy, real-gas air flows can be generated with flow times of about 180 milliseconds. This shock tunnel is operated with a combustion-heated driver gas and consists of a combustion chamber, shock tube, supersonic nozzle, test section, and vacuum tank. An essential feature of this shock tunnel is a means for achieving a constant-pressure air reservoir for the duration of the test. Air streams with velocities in excess of 14,000 feet per second have been achieved at a Mach number of about 10. The corresponding stream total enthalpy is about 4,500 Btu/lb and the stagnation pressure is 3.25 psia.

INTRODUCTION

The shock tunnel has been used extensively to generate high-velocity air flows. The air flow velocities which can be achieved in a shock tunnel depend on the physical dimensions of the apparatus and the nature of the driver gas and the air prior to the initiation of shock compression in the shock tube. In general, for a given shock-tube length, changes in shock-tunnel operation which result in an increase in air velocity will result in a decrease in flow duration. Thus, even though the attainment of high-velocity air flows does provide streams in which models of hypervelocity vehicles can be tested, the testing times may not be sufficiently long for detailed studies of aerodynamic forces, pressures, and heating rates. Consequently, techniques for extending the flow duration of shock tunnels are needed for the continued improvement of these facilities for hypervelocity research.

The mathematical derivation of shock-tube equations, graphs and tables of properties of shock-heated air and the physical description of shock-tube phenomena are given in many publications, including references 1 through 5. Advances in shock-tunnel technology include the use of combustible mixtures of hydrogen and oxygen in helium to attain a

high-energy, low-molecular-weight driver gas (see refs. 6 to 11, for example). Shock compression with a combustion-heated driver gas provides a means for generating air streams at velocities as high as 52,000 feet per second (ref. 8). At velocities ordinarily achievable in shock tunnels (see refs. 8 and 11, for example), flow times vary from about 0.01 to 0.05 millisecond per foot of shock-tube length if special techniques for extending flow times are not used.

Preliminary experimental work at the Ames Research Center led to the development of a technique, called a "one-cycle, shock-compression" process (see appendix A), for extending shock-tunnel flow duration. With this technique, flow times of more than 12 milliseconds per foot of shock-tube length were attained in a small-scale shock tunnel which utilized a cold-helium driver gas (ref. 12). A larger shock tunnel, designed to utilize the same technique, has been constructed at Ames. To attain higher enthalpies, this shock tunnel was designed to utilize a combustion-heated driver gas. The purpose of this report is to describe this shock tunnel and its operation and to present the results of the preliminary calibration of its test stream.

SYMBOLS

a	speed of sound
A	cross-sectional area
d	diameter
h	specific enthalpy
m	molecular weight
M	Mach number
p	pressure
q	rate of heat transfer per unit area
R	gas constant
Re	Reynolds number
t	time
T	absolute temperature
u	velocity

x	distance along axis of shock tube, measured from shock-tube inlet
γ	ratio of specific heats
ρ	density
$(')$	pitot conditions

Subscripts

c	combustion chamber conditions
t	air-reservoir conditions
∞	stream static conditions
$1,2 \ldots 7,8$	state conditions (see fig. 17)

DESCRIPTION OF SHOCK TUNNEL

General Layout

A schematic diagram of the 1-foot hypervelocity shock tunnel and the related test equipment is shown in figure 1. Major components of the shock tunnel are the combustion chamber, shock tube, supersonic nozzle, test section, diffuser, and vacuum tank. The shock tunnel is enclosed by a sand-filled barrier to provide protection to personnel and test equipment from possible explosions or failure of high-pressure fittings. The combustion chamber is supported in a fixed position on a concrete foundation. The rest of the shock tunnel is track-mounted to facilitate separation of the various major components.

Shock Tunnel Components

Photographs of the various components of the shock tunnel are shown in figure 2. The assembled shock tunnel is shown in figure 2(a). The combustion chamber (fig. 2(b)) is 24 feet long with a 27-inch-diameter bore. The shock tube is 40 feet long with a 6.2-inch-diameter bore and is coupled to the combustion chamber with the interrupted-thread breech plug shown in figure 2(c). The supersonic nozzle has a simple conical contour of 9° total angle and is 6.5 feet long with a 1-foot-diameter exit. The nozzle exit can be seen in figure 2(d), a photograph of the 1-foot by 1-foot test section. A diverging diffuser provides flow

transition from the test section into the 500-cubic-foot capacity vacuum tank. A 5-hp vacuum pump is mounted so that the test section complex, consisting of the nozzle, test section, and vacuum tank (fig. 2(e)), can be evacuated before the assembly is coupled to the shock tube.

The various components of the shock tube inlet (see fig. 1 for location) are shown in figure 3. This unit contains a diaphragm that separates the high-pressure gases of the combustion chamber from the air in the shock tube and a punch for initiating diaphragm rupture. In addition, throttling plates with which the flow of these gases into the shock tube is controlled are located in this section. These plates have 7/8-inch-diameter holes with 36 holes in each set, and thus have an open area that is approximately 75 percent of the shock-tube cross-sectional area. Details of the plates, diaphragm, and punch are shown in the sketch of figure 3(a). A photograph of the assembly showing the throttling plates is shown in figure 3(b). The punch (see fig. 3(a)) is shown in detail in figure 3(c). It is driven by an exploding powder charge. The square point of the punch is designed to initiate diaphragm flare in a four-petal pattern. The diaphragm material, shape, and thickness are selected so that upon rupture at a given combustion chamber pressure a complete flare will be achieved. A diaphragm before and after rupture is shown in figure 3(d). This diaphragm was formed from a 0.125-inch-thick sheet of 18-8 stainless steel.

Details of the nozzle inlet (see fig. 1 for location) are shown in figure 4. This section contains a diaphragm which retains the air in the shock tube until shock compression is accomplished. This diaphragm consists of a strip of adhesive-backed cellophane tape and is sufficiently strong to hold a pressure of from two to three atmospheres in the shock tube. The sonic-throat insert is machined from copper and can be removed and replaced if damaged or to change Mach number of flow. Copper is used because it has high thermal conductivity and, thus, good resistance to erosion by surface melting.

Test Equipment

Equipment related to the shock tunnel includes the gas supply system, a gas flow-control system, gas storage and mixing tanks, an ignition system, operating controls, and instrumentation (see fig. 1). This equipment, with the exception of the high-voltage power supply and capacitance bank for the ignition system, is located outside the barrier.

The gases required for shock tunnel operation are stored in cylinders at pressures up to 2,200 pounds per square inch. These gases are helium, hydrogen, and oxygen for the combustion-heated driver gas and dry air for the shock tube. Gases are added to the storage and mixing tanks and the combustion chamber through the gas flow-control system. Ordinarily, the various gases are added to appropriate receivers by direct flow from the

supply, storage, or mixing tanks. However, a 60-hp compressor with a 3,000-psi output can be used to pump helium or the helium-hydrogen mixture when the tank pressures are too low to achieve desired loading pressures.

The ignition system consists of a 20,000-volt power source with a 50-microfarad capacitance bank and 23-foot-long, 0.003-inch-diameter copper-manganese-nickel alloy wires. Six of these wires are mounted lengthwise in the combustion chamber on a 10-inch-diameter circle which is concentric with the chamber axis. Ignition is accomplished by a sudden discharge of the stored electrical energy through the wires. The discharge causes a thermal explosion of the wires which ignites the combustible gas mixture in the chamber.

The shock tunnel operating controls include power circuits, relays, and sequence timers. Controls are provided for safety of personnel and test equipment. Operations are programmed with the sequence timers so that upon initiation of the start signal, all phases are performed automatically. This includes the control of data read-out equipment as well as the operation of the shock tunnel.

OPERATION OF SHOCK TUNNEL

It was previously noted that the 1-foot hypervelocity shock tunnel is operated with a combustion-heated driver gas and was designed to utilize one-cycle shock compression. This shock-compression process and the conditions which must be established if long flow times are to be achieved are discussed in appendix A. Experiments were conducted to determine the conditions best suited for the operation of the shock tunnel and the achievement of long flow times.

Combustion Process

The combustion experiments consisted of a series of tests to determine a suitable ignition technique and the loading conditions which would result in the attainment of a repeatable combustion process with no detonation. The ignition of combustible gas mixtures and the combustion of hydrogen and oxygen when mixed in different proportions with various diluent gases have been discussed in reference 13. Detonation has been discussed extensively in references 13, 14, and 15. It was indicated in reference 13 that even though the proportions and pressures of the combustible mixtures are in a range in which adiabatic combustion can be expected, detonation can be induced if the flame path is long enough for nonisentropic shock compression to occur.

As a result of the data of these references and of the present combustion experiments, the previously described exploding wire ignition system was installed in the shock tunnel. A mixture of gas which consisted (by partial pressure) of 7.2-percent oxygen, 11.8-percent hydrogen, and 81.0-percent helium was found to give satisfactory, repeatable combustion. With a loading pressure of 750 psia, peak combustion chamber pressures of between 4,600 and 5,200 psia were achieved. A typical record, showing the variation of combustion chamber pressure with time, is shown in figure 5. (The sudden drop in pressure occurs when the diaphragm is ruptured and shock compression is initiated.) It was estimated, from equations given in reference 13, that the temperature at the peak pressure was approximately 3,700° R.

Shock-Compression Process

The shock-compression experiments consisted of tests to determine the shock-tube loading pressure and other conditions necessary for one-cycle shock compression. With combustion chamber conditions as specified above, it was estimated (see appendix A) that the desired conditions could be achieved with a pressure ratio across the primary shock wave, or primary-shock-wave strength, of about 105. To attain this shock strength, the calculations indicated that, with the throttling plates previously described, the initial shock-tube pressure should be about 4.1 psia at a temperature of 520° R. Tests were then run with initial shock-tube pressures of 3.4, 3.7, and 4.0 psia. It was found that the one-cycle, shock-compression process was best attained with a pressure of 3.7 psia. A typical record of the pressure rise and subsequent pressure oscillations of the air-reservoir pressure (final shock-tube pressure) is shown in figure 6. A comparison of the combustion chamber pressure record (fig. 5) and the air-reservoir pressure record shows that 100 milliseconds after initiation of shock compression the average pressure in the shock tube is approximately 4,000 psia and is equal to the pressure in the combustion chamber. An examination of figure 6 shows that the pressure oscillations after the completion of shock compression deviate by about ±10 percent from the average pressure. It should be mentioned that, for these tests, the nozzle inlet section was replaced with a closed-end insert which retained the air in the shock tube and which contained a pressure transducer.

CALIBRATION OF SHOCK TUNNEL

Initial calibration tests in the 1-foot hypervelocity shock tunnel were conducted to determine pertinent test stream properties under typical operating conditions. Tests were run with initial loading conditions selected to establish, nominally, a peak combustion chamber pressure of

about 5,000 psia and an average air-reservoir pressure of about 4,000 psia. Usually, peak combustion chamber pressures of between 4,600 and 5,200 psia were attained and resulted in air-reservoir pressures of between 3,800 and 4,200 psia. It should be noted, however, that some of the experimental measurements presented in this report were taken at pressures which deviated appreciably from the nominal values. These tests are reported because the measurements from which useful information could be determined were few in number. Furthermore, data were taken only in the center of the test stream. Consequently, the stream properties presented in this report are considered to be of a preliminary nature.

Experimental Measurements

Test stream properties were evaluated with measured pressures, velocities, and heat-transfer rates. The average flow duration of the test stream was also determined experimentally. In general, separate test runs were required for each stream measurement. A 0.225-inch-diameter sonic throat (see fig. 4) was used for all tests unless otherwise noted.

Stream pressures.- Pitot and static pressures were measured with probes located on the test-section center line and 4 inches downstream of the nozzle exit. Sketches of the pitot- and static-pressure probes are shown in figure 7. Both probes were instrumented with pressure transducers suitable for measuring low-amplitude, high-frequence pressure changes associated with the start of flow in a shock tunnel. The outputs of the pressure transducers were recorded with oscilloscopes. The curves shown in figure 8 were taken from typical oscilloscope records. The oscilloscopes were triggered at the instant the diaphragm punch was activated. The start of flow occurred approximately 8 milliseconds later.

The pitot-pressure record shows an increase to the average maximum level within approximately 2 milliseconds after the start of flow. The average pitot pressure for this test was about 2.8 psia, with deviations estimated to be no more than ±5 percent. The average air-reservoir pressure for this test was about 3,500 psia. The static-pressure record shows a response to the sudden change in pressure at the start of flow, but shows the average maximum level was not reached until about 15 milliseconds after the start of flow. The average static pressure for this test was about 0.021 psia, with deviations estimated to be no more than ±15 percent if the initial peak is ignored. The average air-reservoir pressure for this test was about 4,000 psia.

Stream velocity.- Velocity measurements were made by utilizing the spark-discharge technique discussed in reference 12. Briefly, at a predetermined time after the start of flow, a disturbance was generated in the center of the test stream by an electrical discharge between two electrodes. The disturbance then moved through the test section with

the velocity of the air flow. The disturbance was then photographed with a schlieren apparatus. The time interval between the electrical discharge which caused the disturbance and the schlieren spark discharge was measured with a recording oscilloscope. The distance traveled by the center of the disturbance during this time was determined from the position of the disturbance in the schlieren photograph. The average velocity of the test stream during this time period was determined from the measured distance and the time of travel of the disturbance.

Typical schlieren photographs of the disturbances from which the test stream velocity was determined are shown in figure 9. The two electrodes and a shock probe are also shown in the photographs. In each photograph, the shock wave over the shock probe is indicative of supersonic flow in the test section at the time the photograph was taken. Because it was difficult to generate a single-pulse discharge and thus attain a disturbance with the characteristics of a point source (see ref. 12), sufficient power was used to maintain an electrical discharge for several microseconds. The resulting photographic record shows a pear-shaped disturbance. It was assumed that the spherically shaped leading portion of the disturbance was generated by the first pulse of the spark discharge. The stream velocity was determined from the position of the center of this portion of the disturbance. The photograph shown in figure 9(a) was taken 18 milliseconds after the start of flow. The average velocity at this time was determined to be 13,800 feet per second. At 78 milliseconds after the start of flow (fig. 9(b)), the average velocity was found to be 13,100 feet per second. In both cases, it was estimated that the average velocity could, as a result of inaccuracies in the experimental measurements, deviate by about ±200 feet per second from the stated velocity.

The tests from which the stream velocity was determined were run with a 0.288-inch-diameter sonic throat. Preliminary tests were run with a 0.225-inch-diameter sonic throat, but clearly defined disturbances could not be photographed. This lack of schlieren resolution was attributed to the low density of the high Mach number air flow. The reduction in Mach number through the use of the larger sonic throat doubled the stream density. It was estimated that the decrease in stream velocity due to the decreased Mach number was not more than 150 feet per second and could be neglected.

Heat-transfer rates.- A heat-transfer investigation was included as part of the initial calibration tests. For this investigation, rates of temperature rise were measured at the stagnation point and along the surface of the 3-inch-base-diameter hemisphere shown in figure 10. This model was fabricated from nickel by an electrochemical plating process and had a 0.012-inch-thick skin.

A typical oscillograph record of measured temperature rise as a function of time is shown in figure 11. For these measurements, 10 iron-constantan thermocouples were spot-welded on the inner surface in

locations shown in the same figure. The oscillograph record shows a steady increase in local temperature at each thermocouple with only negligible fluctuations. It should be mentioned that the traces do not represent the same net change in surface temperature at each thermocouple location. For example, for the first 60 milliseconds the net change at thermocouple number 1 (the stagnation point) was approximately 200° Rankine, while the net change at thermocouple number 8 was only 30° Rankine.

Heat-transfer rates were calculated from the measured rates of temperature rise, using the relation that the heat-transfer rate is equal to the product of the specific heat and density of the model skin, the skin thickness at the thermocouple location, and the rate of temperature rise. The resulting heat-transfer rates, accurate to within ±10 Btu/ft^2 sec, are presented as a function of body position in figure 12. For this test, with an air reservoir pressure of 3,500 psia, the stagnation heating rate was found to be about 205 Btu/ft^2 sec.

Flow duration.- Flow times were determined with an optical technique similar to the method reported in reference 12. With this technique, the presence of helium in the test stream was a qualitative indication that the reservoir of air had been expended or that the driver gas had mixed with air in the shock tube. Specifically, a high-voltage arc (10,000 v) between two electrodes was established before the start of flow and maintained throughout the test run. The arc was nearly continuous, with a discharge frequency of about 1 millisecond. Thus, upon initiation of flow, the gas passing through the arc was ionized, with the light output having the characteristic radiation of the gases present in the test stream.

A schematic diagram of the detector equipment is shown in figure 13. A spectrometer was focused on the arc and adjusted to pass the prominent 5875 Å helium line. The light that passed through the spectrometer was amplified with a photomultiplier. A continuous record of the output of the photomultiplier was taken with recording oscilloscopes set in series to record for several hundred milliseconds. A reproduction of the photomultiplier output trace is shown in figure 14. The increase in the photomultiplier output 180 milliseconds after the start of flow indicated the onset of helium flow through the test section.

Flow times determined with the arc discharge technique are in good agreement with calculated values. For example, a flow duration of 200 milliseconds was expected with the 0.225-inch-diameter sonic throat used for this test. This value was determined from the mass flow rate through the nozzle, calculated for an isentropic expansion from the reservoir, and the mass of air in the shock tube before initiation of shock compression.

Test Stream Properties

Test stream properties were calculated from measured stream pressures and velocities by use of the adiabatic flow equations of conservation of mass, energy, and momentum and the thermodynamic charts presented in references 5 and 16. It was assumed that the air in the test stream was in chemical equilibrium and that the thermodynamic and transport properties of air presented in references 17 and 18 were applicable.

It was previously noted that peak combustion chamber pressures attained in the present calibration tests varied considerably from the nominal value of 5,000 psi. Consequently, operation of the shock tunnel with a fixed initial shock tube pressure (3.7 psia) resulted in variations in air-reservoir and test-stream pressures. Experimental values of pitot and static pressures from several test runs are shown in figure 15. (The shaded areas represent the limits of uncertainty of these measurements.) It was assumed that, for a given Mach number, the stream pressures were proportional to the air-reservoir pressures. Thus, the curves, faired through the experimental data, represent the values of these pressures as a function of air-reservoir pressure at the start of flow.

Variations in combustion chamber pressure also resulted in variations in air-reservoir enthalpy and, therefore, in variations in stream total enthalpy and velocity. The deviation in air-reservoir enthalpy with respect to the deviation in air-reservoir pressure (calculated with shock-tube equations for the noted pressure range) was estimated to be about 0.975 Btu/lb per psi. It was assumed that this relation could be used to determine the stream total enthalpy at the start of flow for tests in which the nominal combustion chamber pressure and, hence, the nominal air-reservoir pressure was not achieved. It was further assumed that the stream total enthalpy decreased exponentially with flow time because of heat losses in the air reservoir and nozzle. The values of pitot and static pressure (from fig. 15) corresponding to the experimental value of air-reservoir pressure for each test were used to calculate the stream static and total enthalpies for each of the measured velocities.

An empirical equation, in which the above deviation (0.975 Btu/lb per psi) was utilized, was developed to fit these calculated stream total enthalpies. This equation and the curves showing the calculated variations of stream total enthalpy with flow time for the two measured velocity runs are shown in figure 16 along with a curve for the nominal air-reservoir pressure of 4,000 psia. For the nominal value of air-reservoir pressure, the nominal value of stream total enthalpy was calculated to be 4,500 Btu/lb at the start of flow. The corresponding nominal value of stream velocity was calculated to be 14,600 feet per second. These and other pertinent nominal stream properties are compiled in table I.

The measured heat-transfer rates were used to substantiate the stream properties measured. For this, the experimental stagnation-point heating rate was compared with that which would be calculated with the theory of reference 19. For this calculation, the experimentally derived nominal stream properties were used (adjusted to the test air-reservoir pressure of 3,500 psi). The result of this calculation indicated that the stagnation-point heating rate should be about 200 Btu/ft^2 sec. This result agrees with the experimental value within the accuracy of the measurement (see fig. 12). Since the theory of reference 19 has been shown by others to agree with experiments (see, e.g., ref. 20) the agreement between the present experimental and theoretical heat-transfer rates was considered to be a good indication that the stream properties were correctly evaluated.

Ames Research Center
National Aeronautics and Space Administration
Moffett Field, Calif., June 4, 1962

APPENDIX A

THE ONE-CYCLE SHOCK-COMPRESSION PROCESS

The "one-cycle shock-compression" process is a nonisentropic compression process which eliminates the pressure and temperature fluctuations in the air reservoir of a shock tunnel. The conditions pertinent to the achievement of this process in the Ames 1-Foot Hypervelocity Shock Tunnel were calculated with the analytical method of reference 12 and with real-gas shock-tube equations similar to those presented in reference 2. The wave diagram depicted in figure 17 helps visualize the various steps necessary to the achievement of the one-cycle shock-compression process. Shock compression of the air in the shock tube (state 1) is initiated by the sudden release of the driver gas (state 4) upon rupture of the diaphragm which separates the combustion chamber and shock tube. The driver gas expands into the shock tube at a rate which is influenced by its pressure and energy, the geometry of the shock-tube inlet, and the pressure and energy of the air in the shock tube. The primary-shock-wave strength is maintained as the air (state 2) is driven by the high-velocity driver gas (state 3) toward the nozzle end of the shock tube at a supersonic velocity. The reflected shock wave is formed when the primary shock wave reaches the end of the shock tube. It moves back toward the combustion chamber as the forward motion of the air is stopped. The air is, by this process, compressed nonisentropically to a high temperature and pressure (state 5).

As soon as the primary shock wave reaches the nozzle end of the shock tube, the nozzle diaphragm (see figs. 1 and 4) is broken by the compressed air. The high-pressure air in state 5 then expands to a high velocity in the nozzle and flows through the test section and diffuser into the vacuum tank. Air flow through the nozzle continues while the reflected shock wave moves toward the combustion chamber. Since the sonic-throat diameter is much smaller than the shock-tube-bore diameter, it is assumed that this nozzle air flow does not modify the shock compression process.

To attain the one-cycle shock-compression process, it is required that no pressure fluctuations or disturbances influence the condition of the air reservoir (state 5). Now, as the reflected shock wave moves from the air into the driver gas, it is required that no disturbances be generated by the interaction of the reflected shock wave and the contact surface. This requirement can be satisfied if the driver gas can also be brought to rest, in state 6. This can be done if the reflected shock wave compresses the gases in states 2 and 3 to the same pressure in states 5 and 6 ($p_5 = p_6$).

It is further required that expansion waves that occur in the combustion chamber must not generate strong disturbances which can enter the shock tube. Such expansion waves will be weak if the combustion chamber is much larger in volume than the shock tube. Therefore, disturbances generated by these expansion waves will also be weak and, thus, have very little influence on the gases in the shock tube.

Finally, it is required that no expansion or compression waves be generated as the reflected shock wave enters the combustion chamber. Such waves will occur if, at this time, the pressure of the driver gas in the combustion chamber (state 8) is not equal to the pressure of the driver gas in the shock tube (state 6). This requirement can be satisfied if equilibrium pressure ($p_8 = p_6$) can be established across the shock-tube inlet.

In the small-scale shock tunnel described in reference 12, the above requirements were satisfied by operation with properly selected combustion-chamber and shock-tube volumes, initial loading conditions, and, a special feature, throttling plates located in the shock-tube inlet. The 1-foot hypervelocity shock tunnel design was based on this concept of operation. The results of calculations to determine the design dimensions and to estimate the performance capability of this shock tunnel are presented in figure 18. Driver-gas properties used in these calculations were estimated with the equations given in reference 13.

The pressure ratios, p_8/p_4 and p_5/p_4, are shown as a function of the primary-shock-wave strength, p_2/p_1, for various values of the initial temperature ratio, T_4/T_1, in figure 18(a). For a given T_4/T_1, the point of intersection of the pressure ratio curves occurs at the values of p_8/p_4, p_5/p_4, and p_2/p_1 for which $p_5 = p_6 = p_8$, and, hence, one-cycle shock compression is achieved. The combustion-chamber volume is calculated with the indicated value of p_8/p_4 and a given shock-tube volume. The throttling plates are selected (based on the required mass-flow rate of the driver gas and the combustion-chamber and shock-tube cross-sectional areas) to result in the required primary-shock-wave strength, p_2/p_1, and, hence, air-reservoir pressure, p_5. For example, for the present tests, with a combustion chamber pressure, p_4, of about 4,800 psi, the temperature ratio, T_4/T_1, was estimated to be approximately 7.1. For this value, the primary-shock-wave strength was expected to be about 105, with a resulting air-reservoir pressure, p_5, of about 4,300 psi.

Now, the properties of the air reservoir (state 5) can be related to the strength of the primary shock wave and the initial pressure, density, and enthalpy of the air in the shock tube. This relationship is illustrated with figure 18(b), a plot of air-reservoir properties as a function of the primary-shock-wave strength, p_2/p_1. The initial conditions are related by the equations

$$\frac{p}{\rho} = \frac{\gamma - 1}{\gamma} h = RT$$

Thus, the initial conditions required for the attainment of one-cycle shock compression can be found at the previously estimated shock strength, $p_2/p_1 = 105$, and the estimated value of the air-reservoir pressure, $p_5 = 4{,}300$ psia. At this value of p_2/p_1, the pressure ratio, p_5/p_1, is found to be about 1,050. Thus, it was estimated that an initial pressure, p_1, of about 4.1 psia at a temperature, T_1, of 520° Rankine was required for the desired shock-compression process.

REFERENCES

1. Glass, I. I., Martin, W., and Patterson, G. N.: A Theoretical and Experimental Study of the Shock Tube. UTIA Rep. No. 2, Univ. of Toronto, Inst. of Aerophysics, Nov. 1953.

2. Feldman, Saul: Hypersonic Gas Dynamic Charts for Equilibrium Air. AVCO Res. Lab., Research Rep. 40, Jan. 1957.

3. Jones, Jim J.: Experimental Investigation of Attenuation of Strong Shock Waves in a Shock Tube with Hydrogen and Helium as Driver Gases. NACA TN 4072, 1957.

4. Martin, W. A.: A Review of Shock Tubes and Shock Tunnels. Convair Rep. No. ZR-658-050, Sept. 1958.

5. Glass, I. I., and Hall, J. Gordon: Handbook of Supersonic Aerodynamics, Section 18, Shock Tubes. NAVORD Rep. 1488 (vol. 6), Bureau of Naval Weapons.

6. Hertzberg, A., Smith, W. E., Glick, H. S., and Squire, W.: Modifications of the Shock Tube for the Generation of Hypersonic Flow. Rep. AD-789-A-2, Cornell Aero. Lab., March 1955. (Arnold Eng. Dev. Ctr. TN 55-15.)

7. Hertzberg, A.: The Shock Tunnel and Its Applications to Hypersonic Flight. Rep. AD-1052-A-5, Cornell Aero. Lab., June 1957. (Office of Scientific Research TN 57-268.)

8. Nagamatsu, H. T., Geiger, R. E., and Sheer, R. E., Jr.: Hypersonic Shock Tunnel. ARS Jour., vol. 29, no. 5, May 1959, pp. 332-340.

9. Seigel, A. E., and Slawsky, Z. I.: A Hypervelocity Gun Using a Shock-Compressed Steam-Heated Propellant. NAVORD Rep. 4345, 1956. (Also Naval Ordnance Lab. Aeroballistic Research Rep. 351.)

10. Nagamatsu, H. T., and Martin, E. D.: Combustion Investigation in the Hypersonic Shock Tunnel Driver. G. E. Res. Lab. Rep. No. 58-RL-2092, Oct. 1958.

11. Wittliff, Charles E., Wilson, Merle R., and Hertzberg, Abraham: The Tailored-Interface Hypersonic Shock Tunnel. Jour. Aero. Sci., vol. 26, no. 4, April 1959, pp. 219-228.

12. Cunningham, Bernard E., and Kraus, Samuel: Experimental Investigation of the Effect of Yaw on Rates of Heat Transfer to Transverse Circular Cylinders in a 6500-Foot-Per-Second Hypersonic Air Stream. NACA RM A58E19, 1958.

13. Lewis, Bernard, and von Elbe, Guenther: Combustion, Flames and Explosions of Gases. Academic Press, Inc., N. Y., 1951.

14. Oppenheim, A. K., and Stern, R. A.: On the Development of Gaseous Detonation. I. Appraisal of the Problem. Tech. Note DR. I. Univ. of Calif., June 1958. (Office of Scientific Research TN 58-383.)

15. Gross, R. A., and Oppenheim, A. K.: Recent Advances in Gaseous Detonation. ARS Jour., vol. 29, no. 3, March 1959, pp. 173-179. (Also Office of Scien. Res. TN 58-893 and Amer. Rocket Soc. paper 688-58.)

16. Moeckel, W. E., and Weston, Kenneth C.: Composition and Thermodynamic Properties of Air in Chemical Equilibrium. NACA TN 4265, 1958.

17. Hilsenrath, J., and Beckett, C. W.: Tables of Thermodynamic Properties of Argon-Free Air to 15,000°K. AEDC-TN-56-12, Arnold Eng. Dev. Ctr., Sept. 1956. (Also AEDC MIPR-AEDC-1.)

18. Hansen, C. Frederick: Approximations for the Thermodynamic and Transport Properties of High Temperature Air. NASA TR R-50, 1959.

19. Fay, J. A., and Riddell, F. R.: Theory of Stagnation Point Heat Transfer in Dissociated Air. Jour. Aero. Sci., vol. 25, no. 2, Feb. 1958, pp. 73-85 (also Avco Res. Rep 121).

20. Rose, P. H., and Stark, W. I.: Stagnation Point Heat-Transfer Measurements in Dissociated Air. Jour. Aero. Sci., vol. 25, no. 2, Feb. 1958, pp. 86-97.

TABLE I.- NOMINAL TEST STREAM PROPERTIES

Air-reservoir pressure, p_t	4,000 ± 200, psia
Pitot pressure, p'	3.25 ± 0.15, psia
Static pressure, p_∞	0.023 ± 0.003, psia
Velocity, u_∞	14,600 ± 500, ft/sec
Mach number, M_∞	10.0 ± 0.4
Reynolds number per foot, Re_∞/ft	59,000 ± 5,000, 1/ft

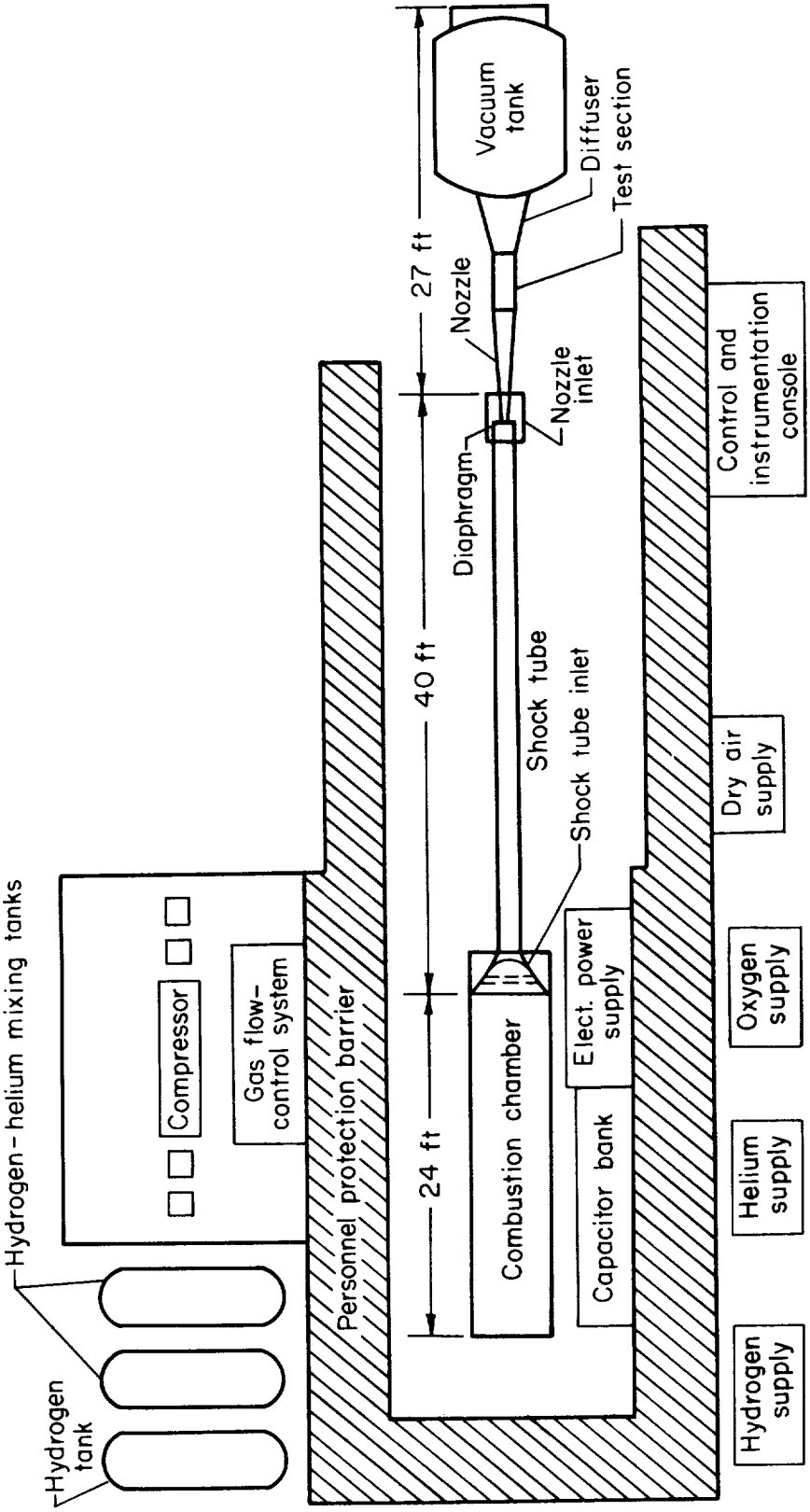

Figure 1.- Schematic diagram of the Ames 1-Foot Hypervelocity Shock Tunnel.

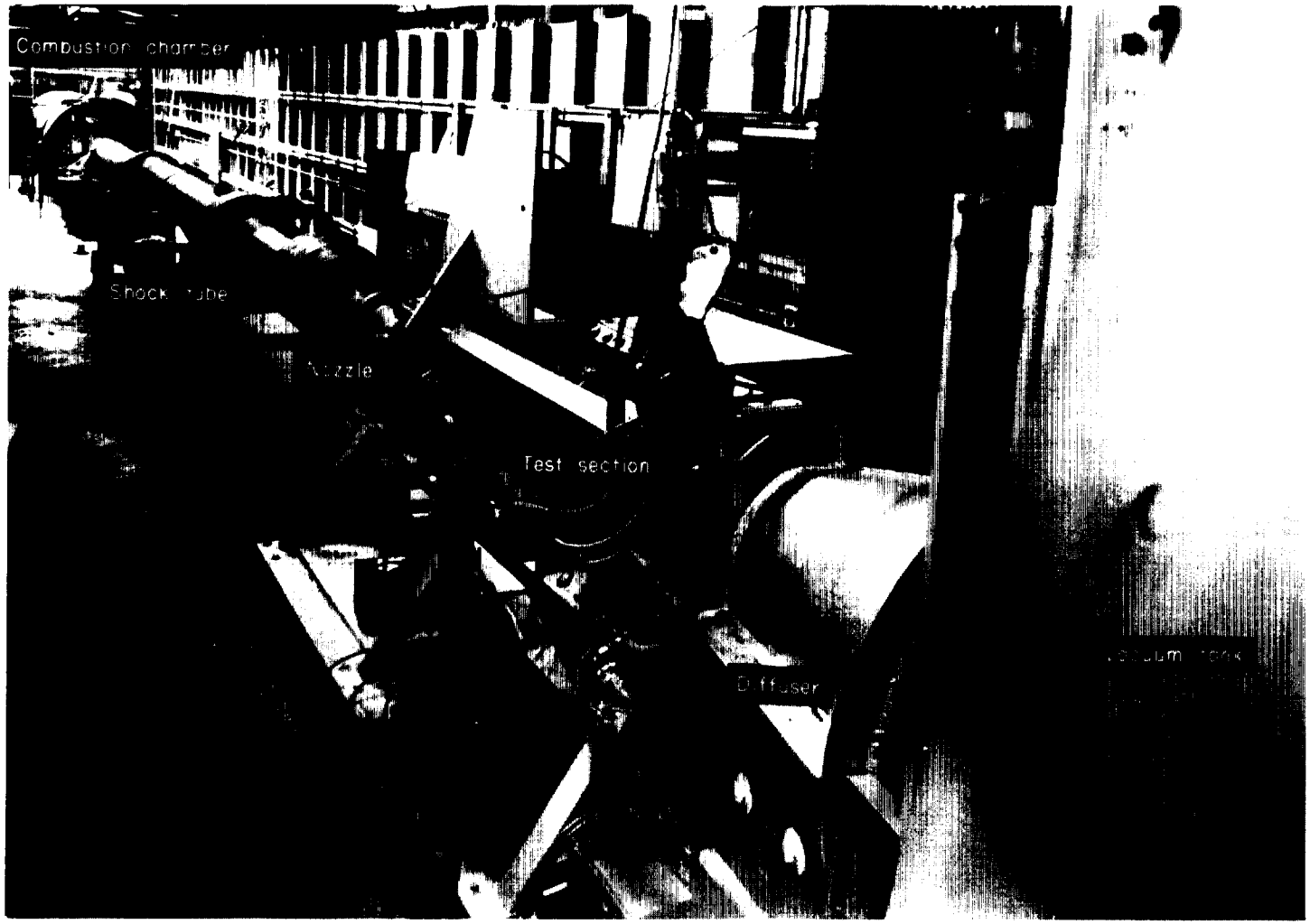

A-26888.1

(a) Assembled shock tunnel.

Figure 2.- Detailed photographs of the Ames 1-Foot Hypervelocity Shock Tunnel.

A-26889

(b) Combustion chamber.

Figure 2.- Continued.

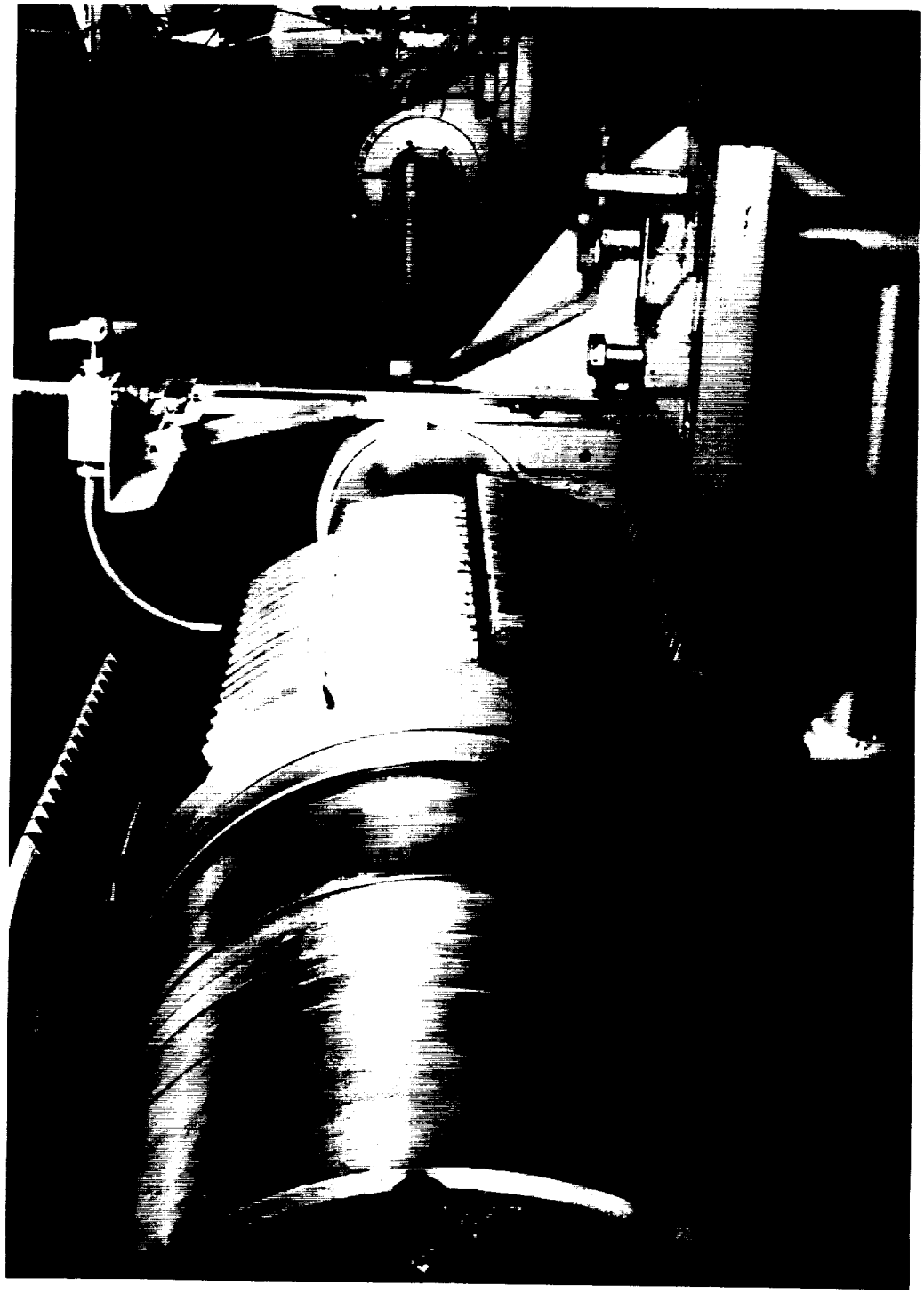

A-26890

(c) Shock tube.

Figure 2.- Continued.

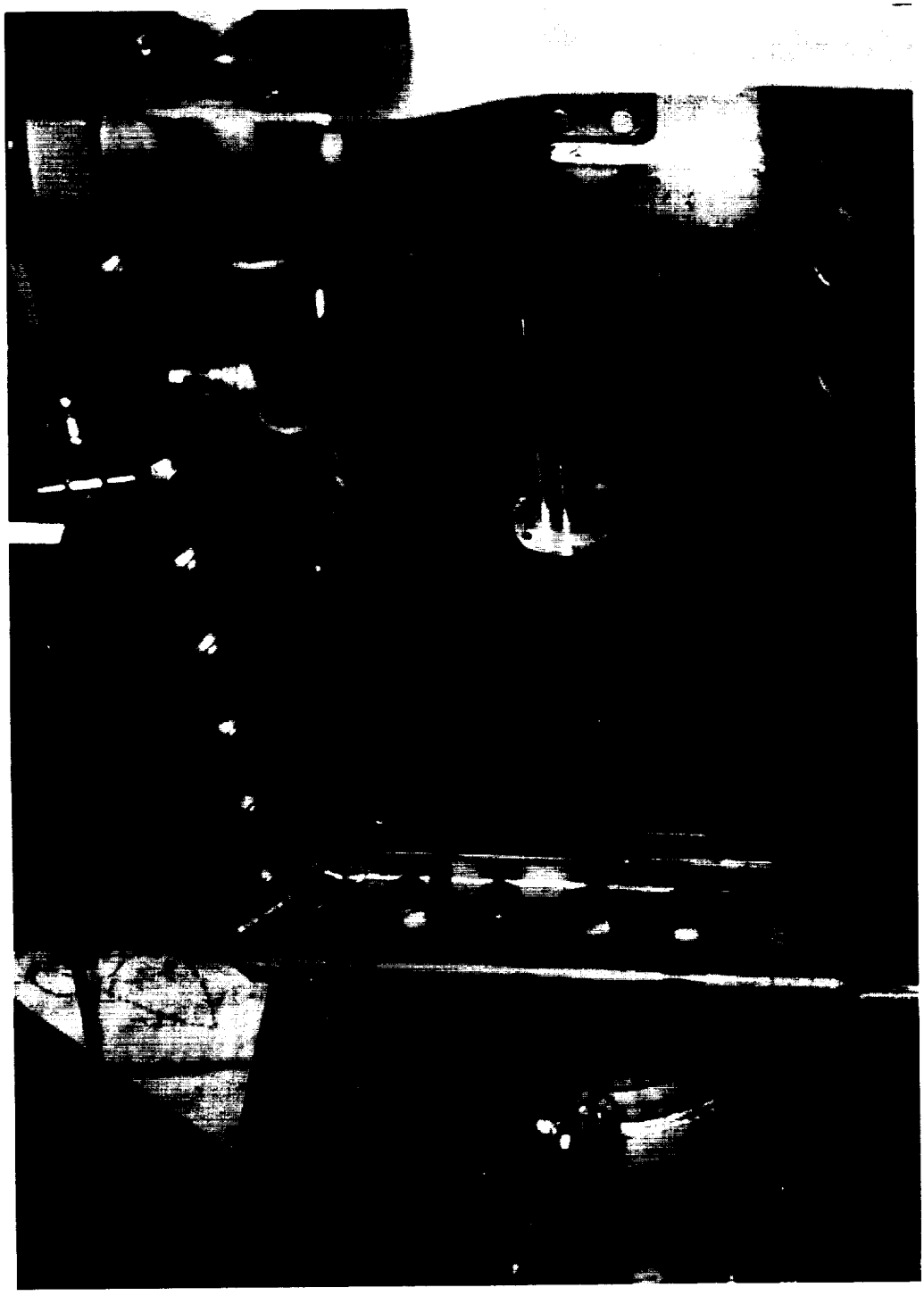

A-26891

(d) Test section.

Figure 2.- Continued.

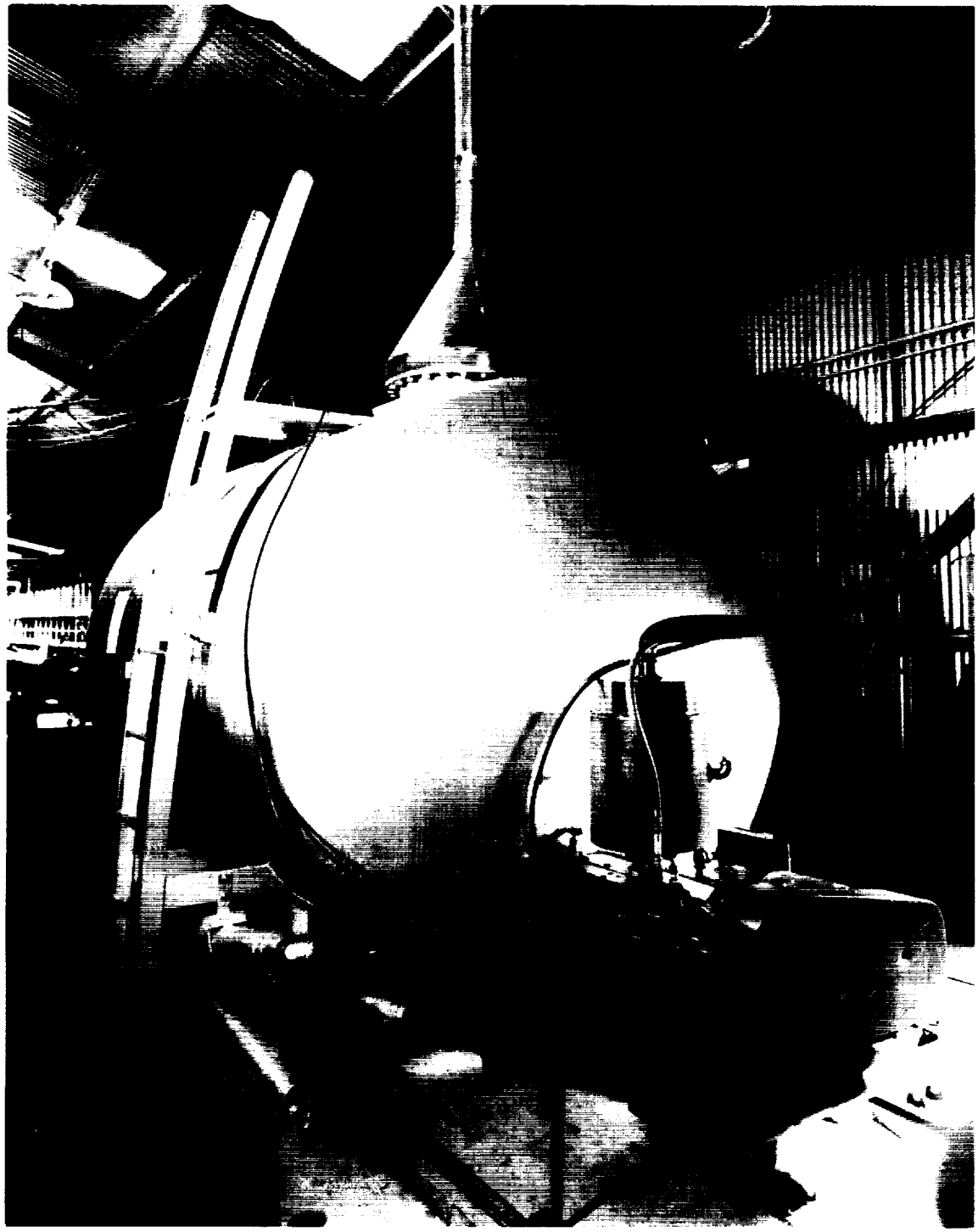

(e) Vacuum tank. A-26892

Figure 2.- Concluded.

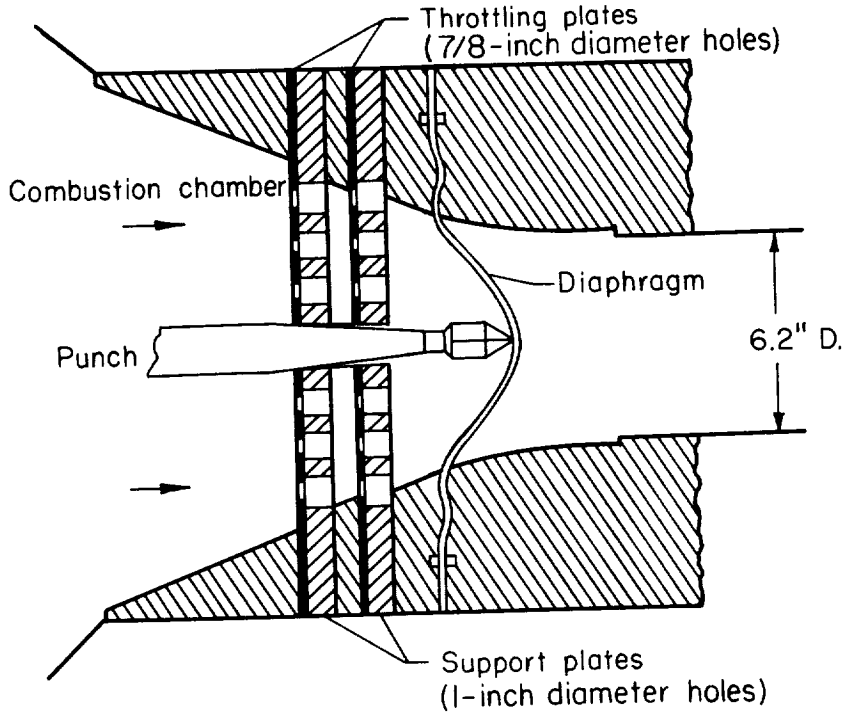

(a) Schematic diagram showing punch, throttling plates, and diaphragm.

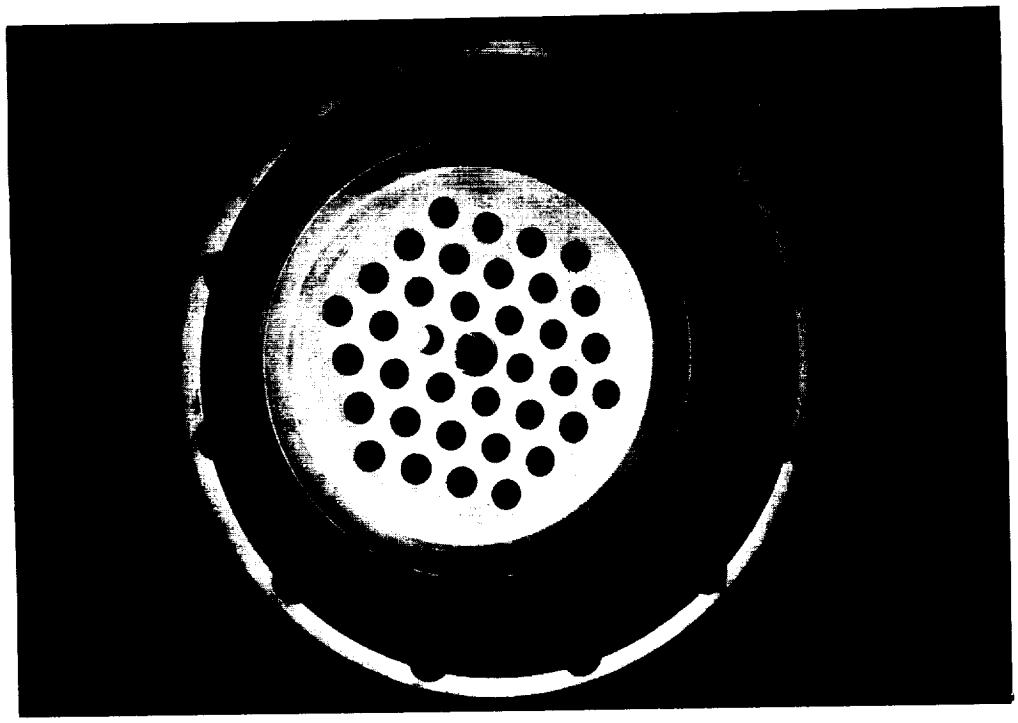

A-26893

(b) Throttling plates.

Figure 3.- Components of the shock-tube inlet.

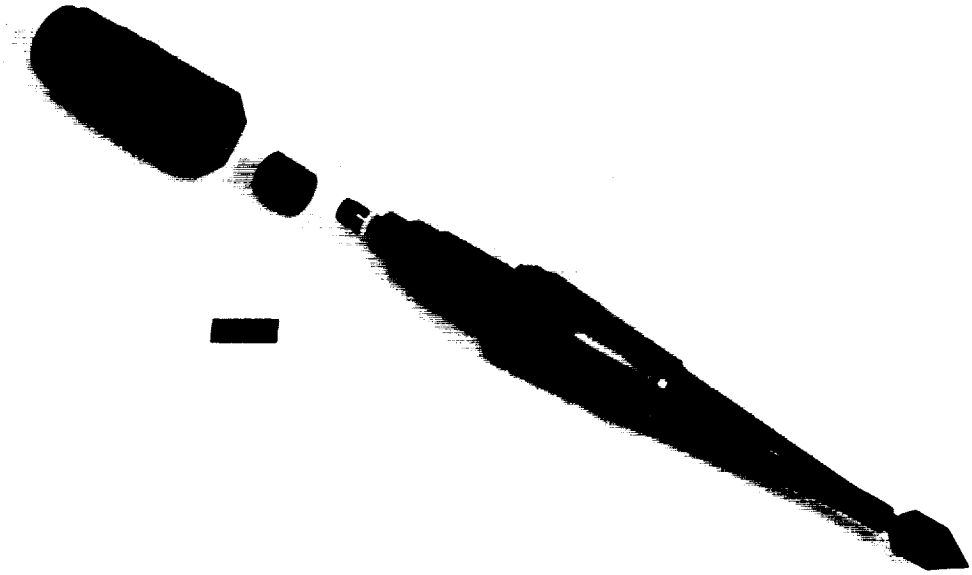

(c) Punch assembly. A-26894

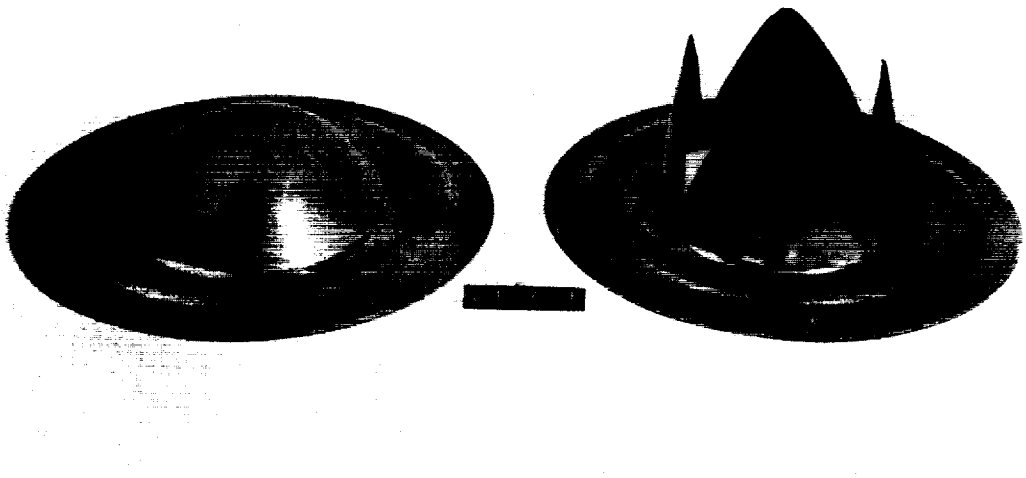

(d) Shape of diaphragm before and after rupture. A-26895

Figure 3.- Concluded.

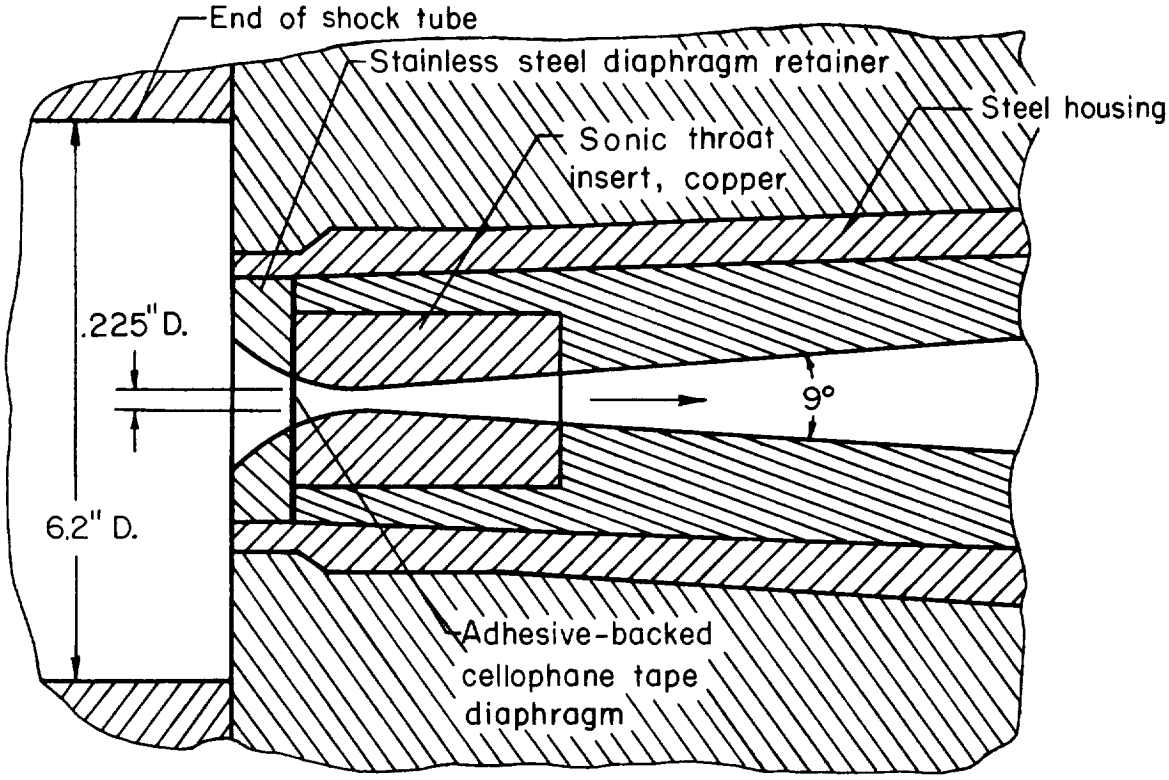

Figure 4.- Sketch of nozzle inlet.

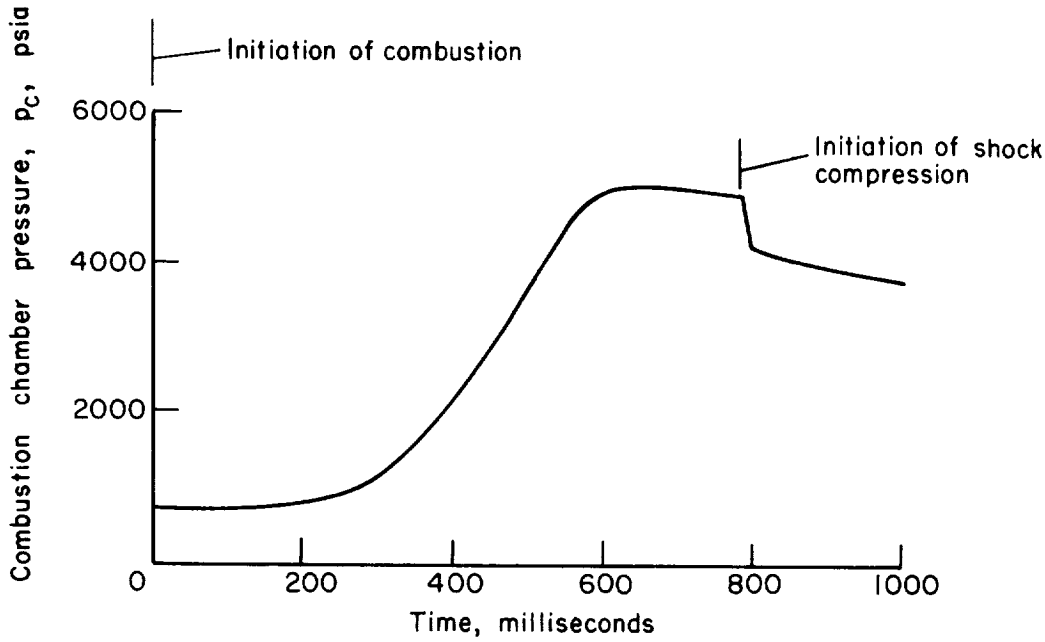

Figure 5.- Variation of combustion chamber pressure after initiation of combustion.

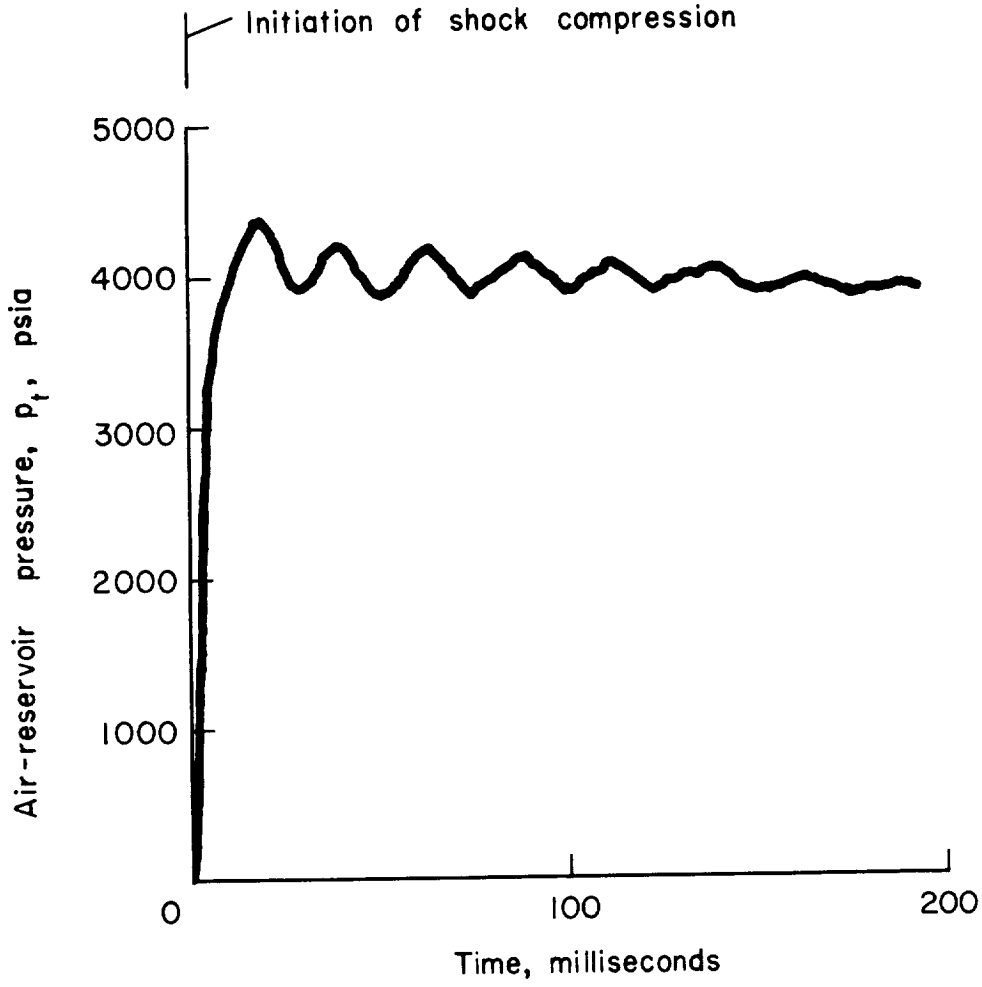

Figure 6.- Variation of air-reservoir pressure after initiation of shock compression.

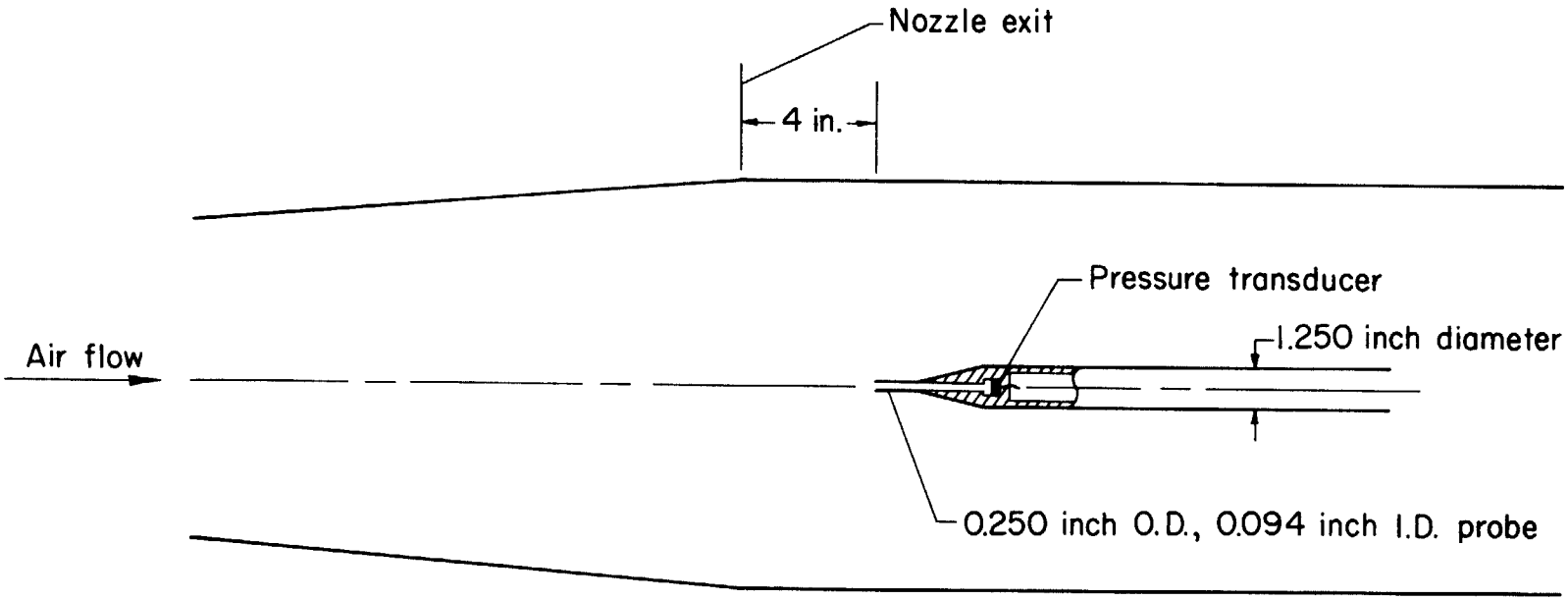

(a) Pitot-pressure probe.

Figure 7.- Schematic diagram of pressure probes in test section of shock tunnel.

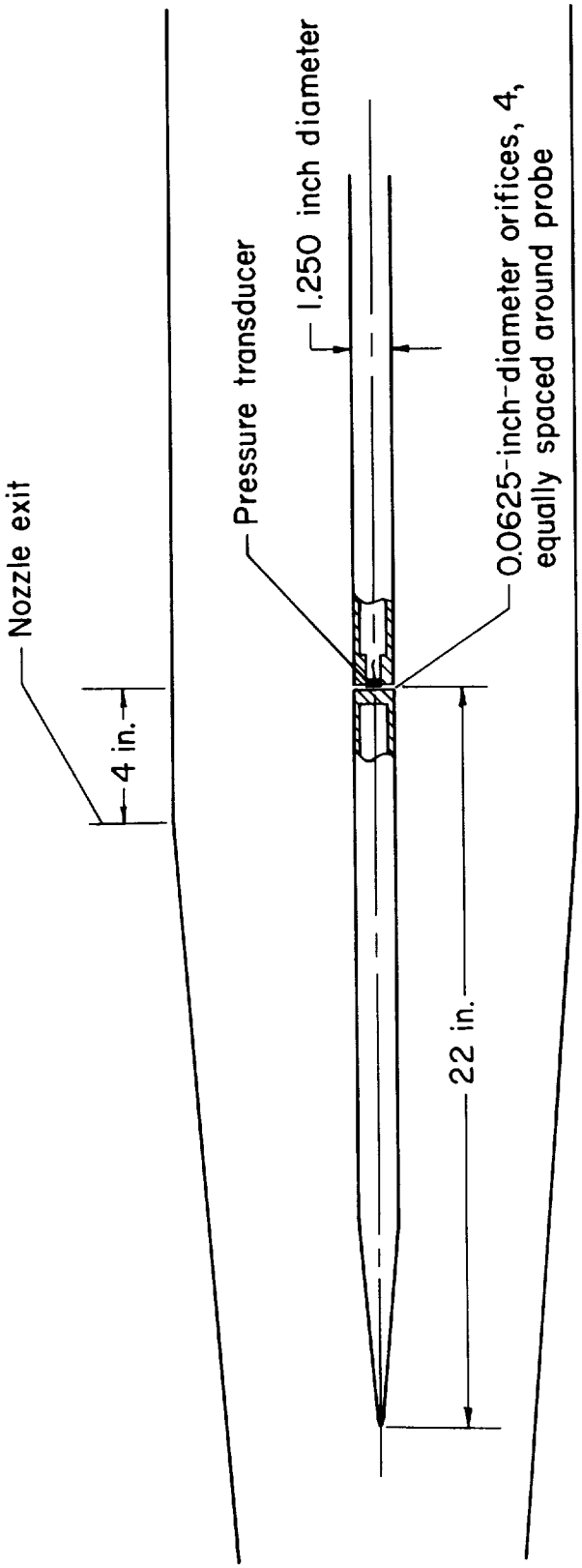

(b) Static-pressure probe.

Figure 7.- Concluded.

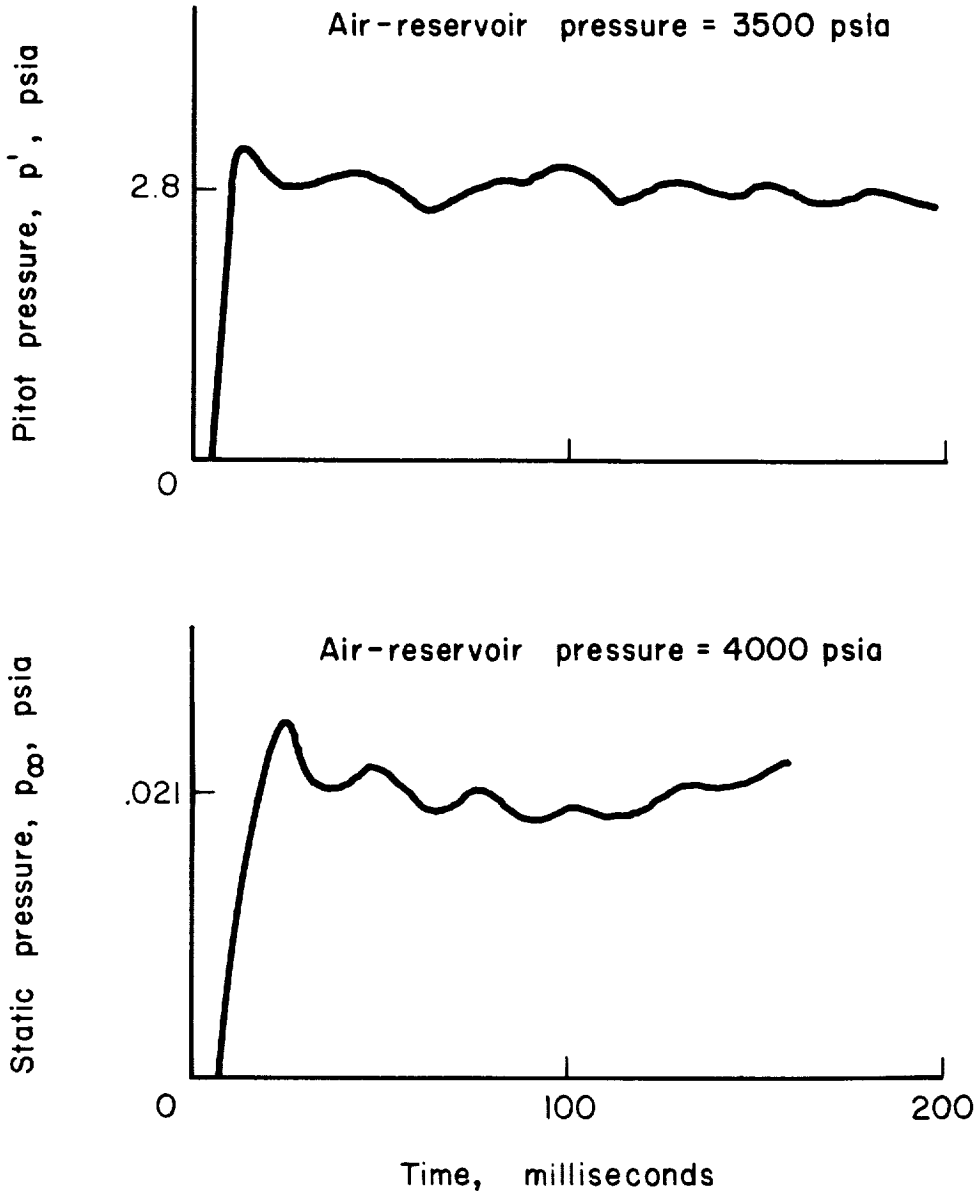

Figure 8.- Variation of stream pressures after start of air flow.

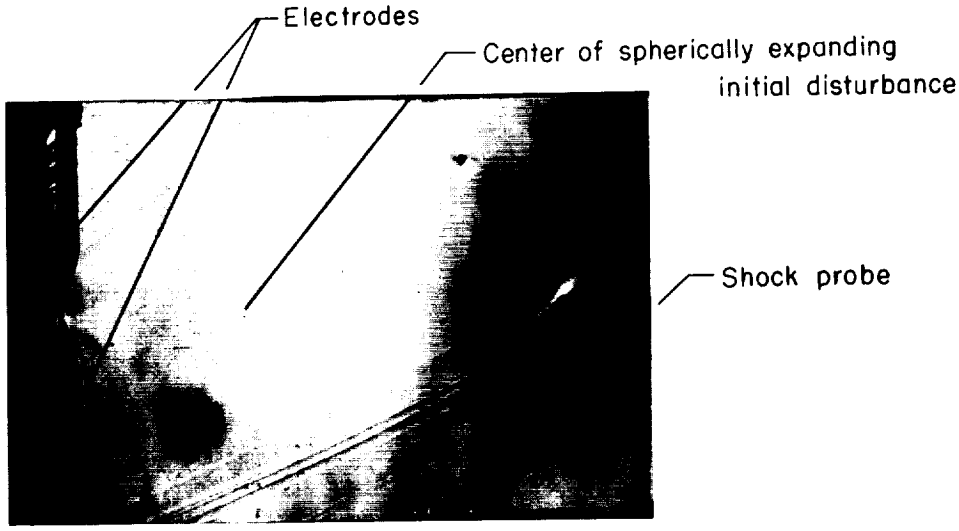

(a) 16 milliseconds after start of flow; time interval between disturbance and schlieren spark discharges, 21.5 microseconds.

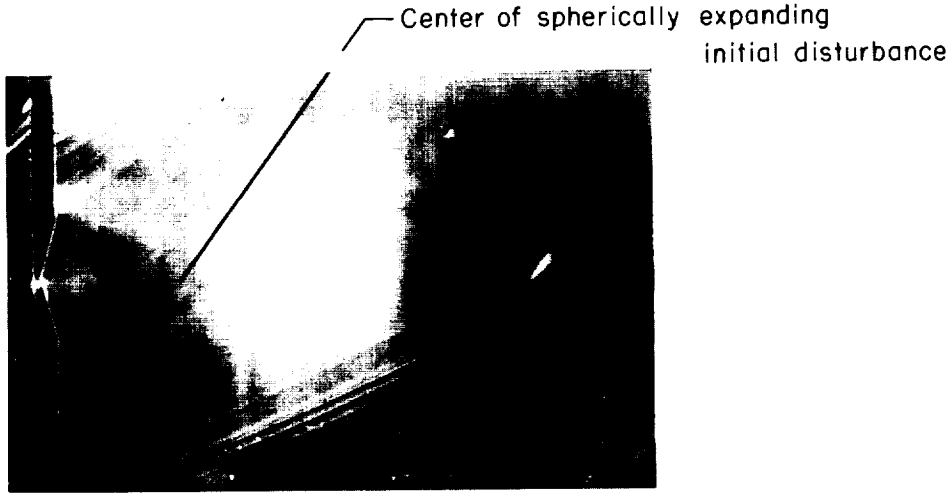

(b) 78 milliseconds after start of flow; time interval between disturbance and schlieren spark discharges, 17.4 microseconds.

Figure 9.- Schlieren photographs from which the average stream velocity at a given time after the start of flow is determined.

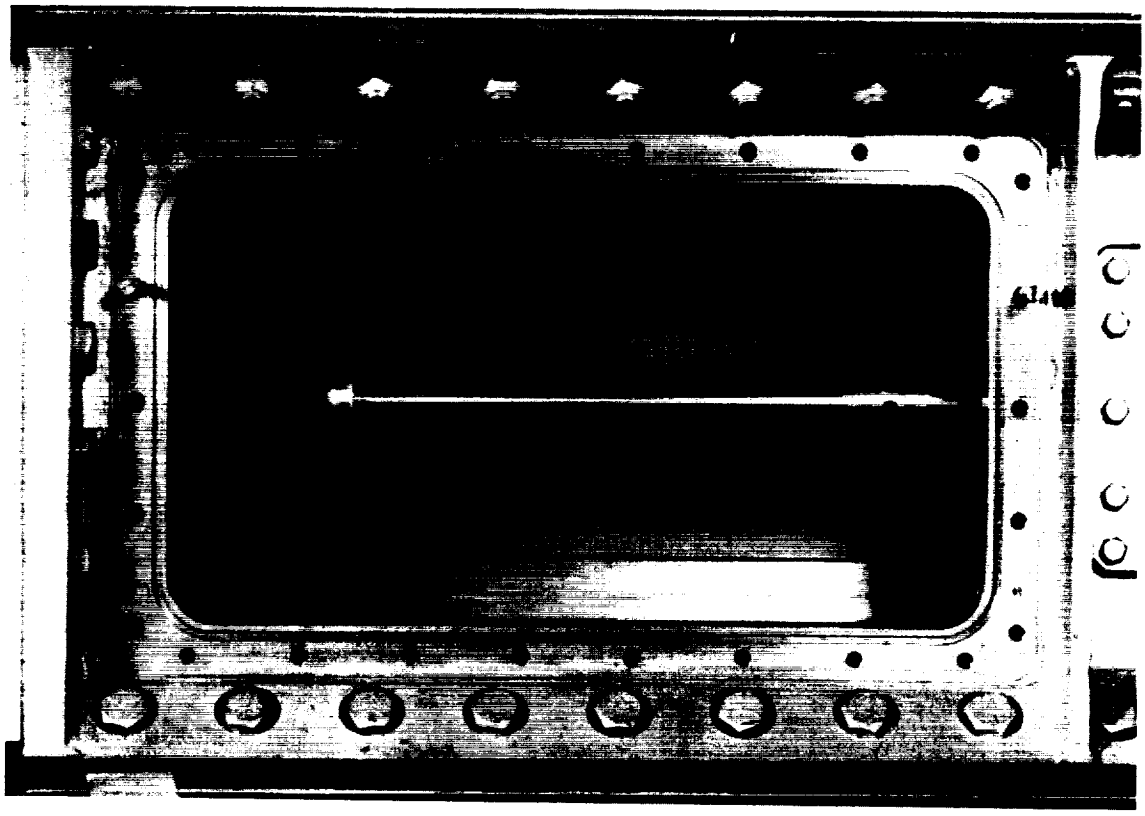

A-27067

Figure 10.- Photograph of heat-transfer model mounted in test section of shock tunnel (3-inch-base-diameter hemisphere).

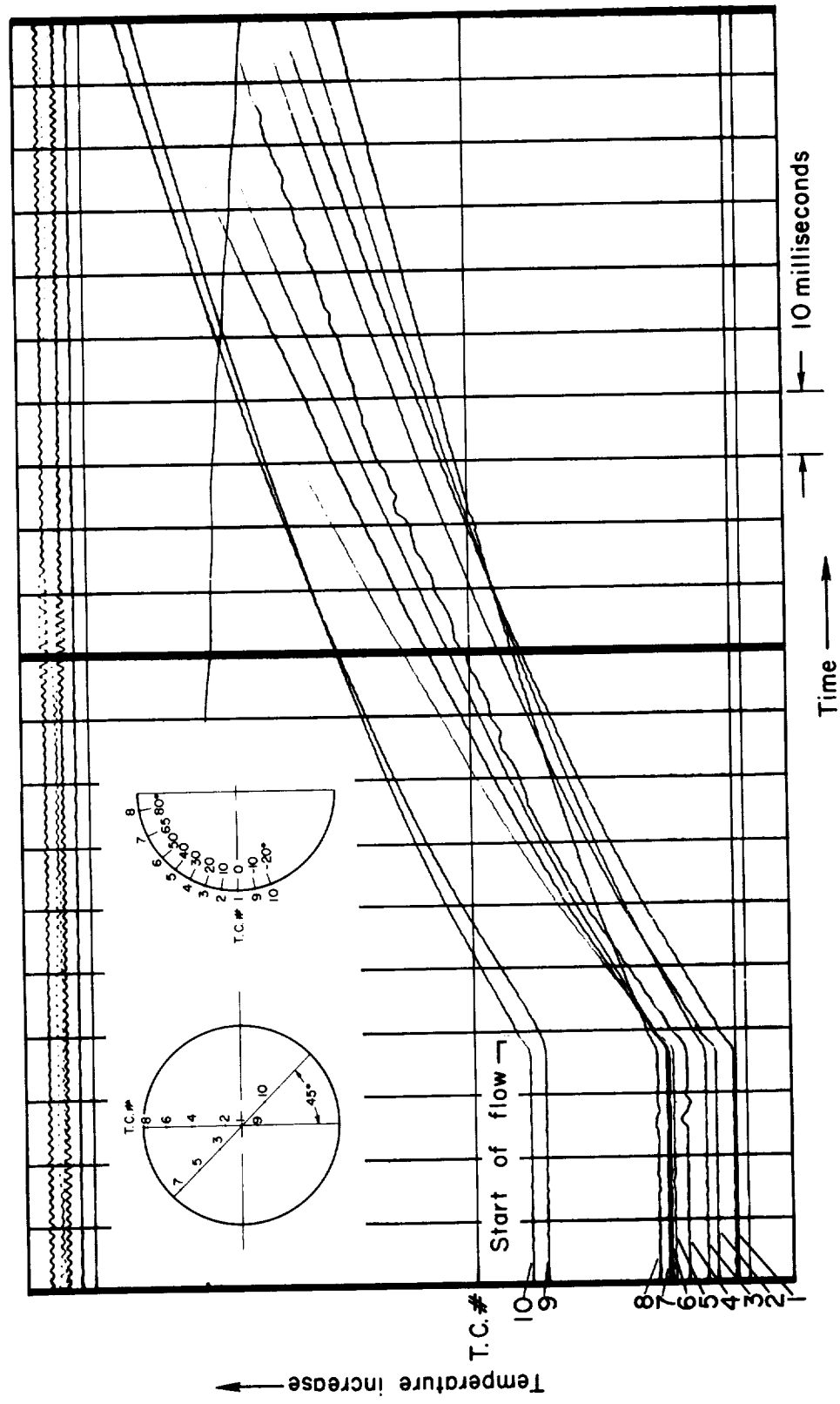

Figure 11.- Typical oscillograph record of temperature rise of 3-inch-base-diameter hemisphere during run.

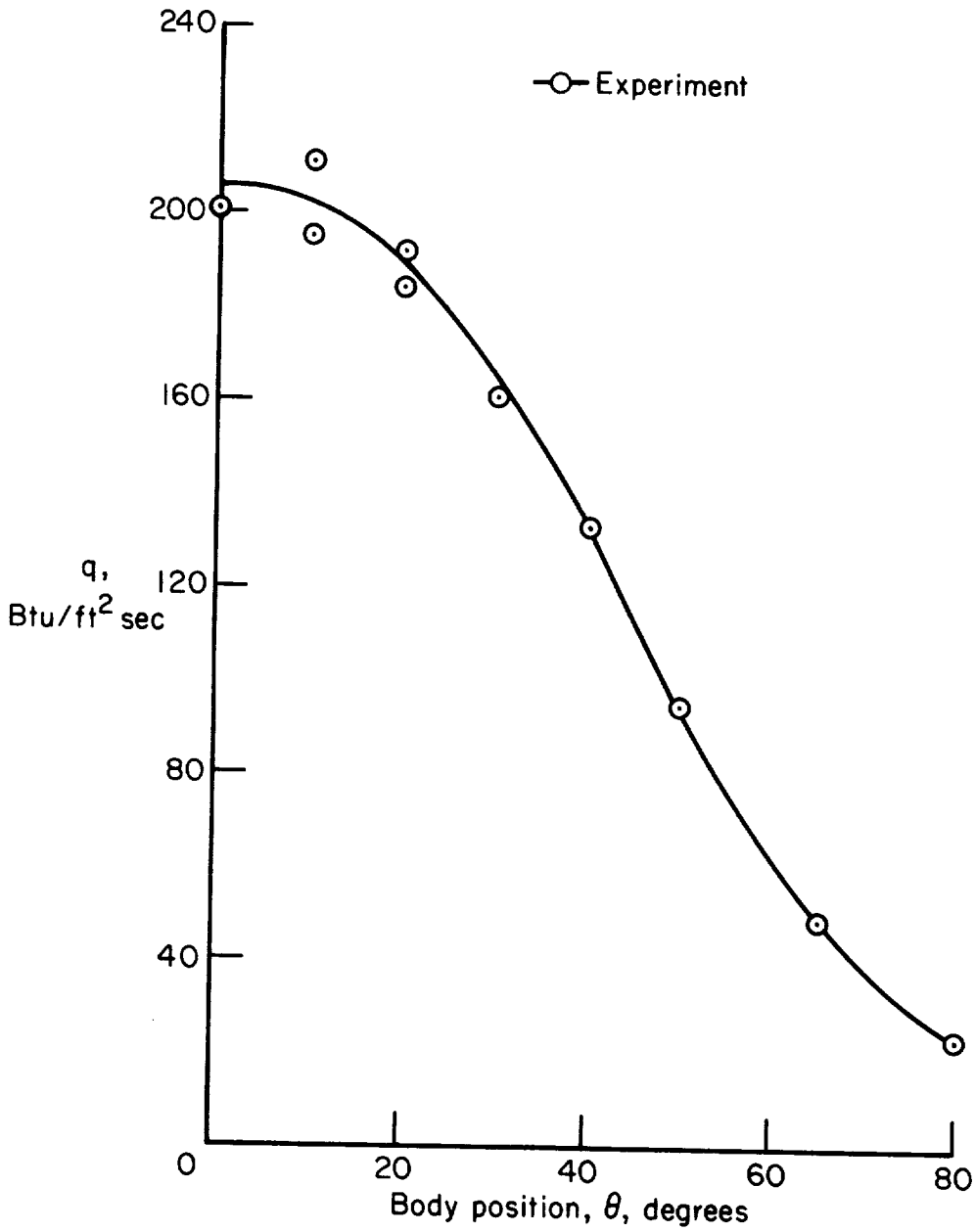

Figure 12.- Local rates of heat transfer to a 3-inch-base-diameter hemisphere (air-reservoir pressure, p_t = 3,500 psia).

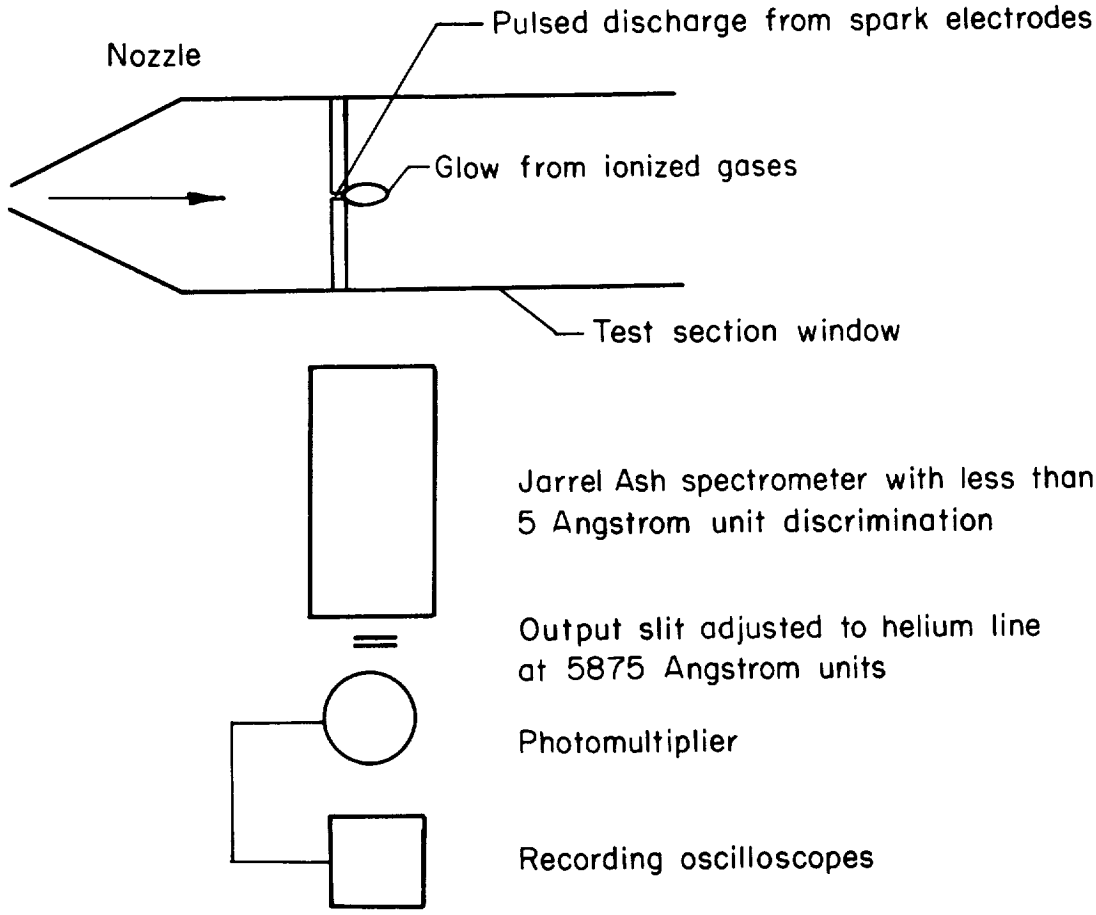

Figure 13.- Schematic diagram of the helium detector equipment.

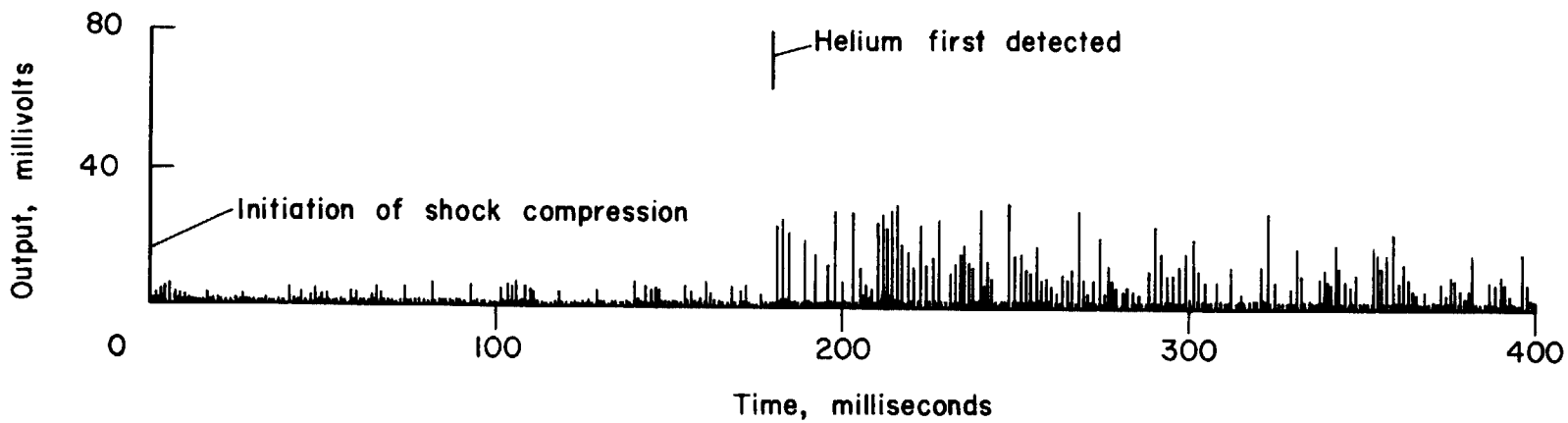

Figure 14.- Variation of output of helium detector after start of flow.

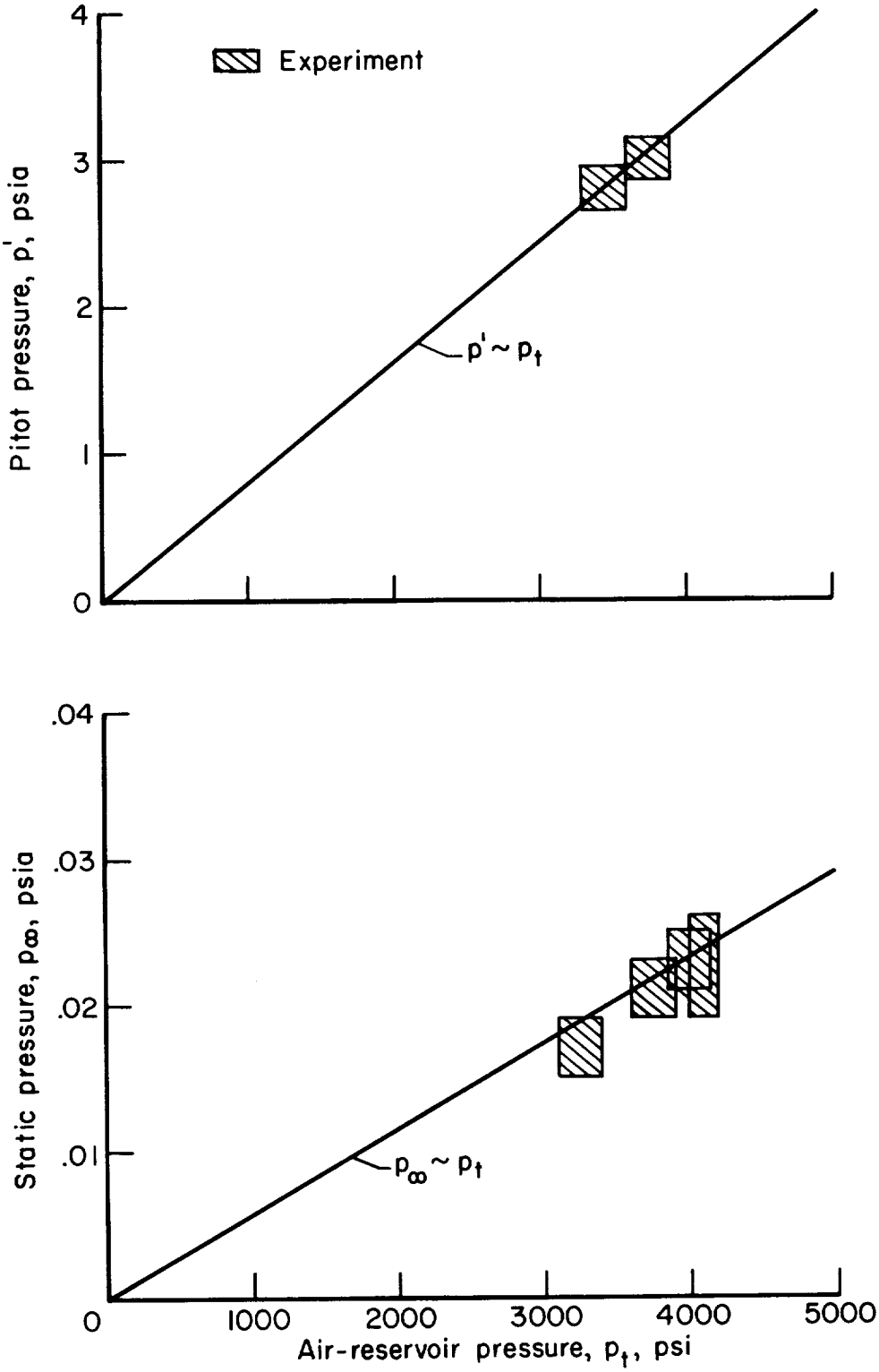

Figure 15.- Variation of pitot and static pressures with air-reservoir pressure.

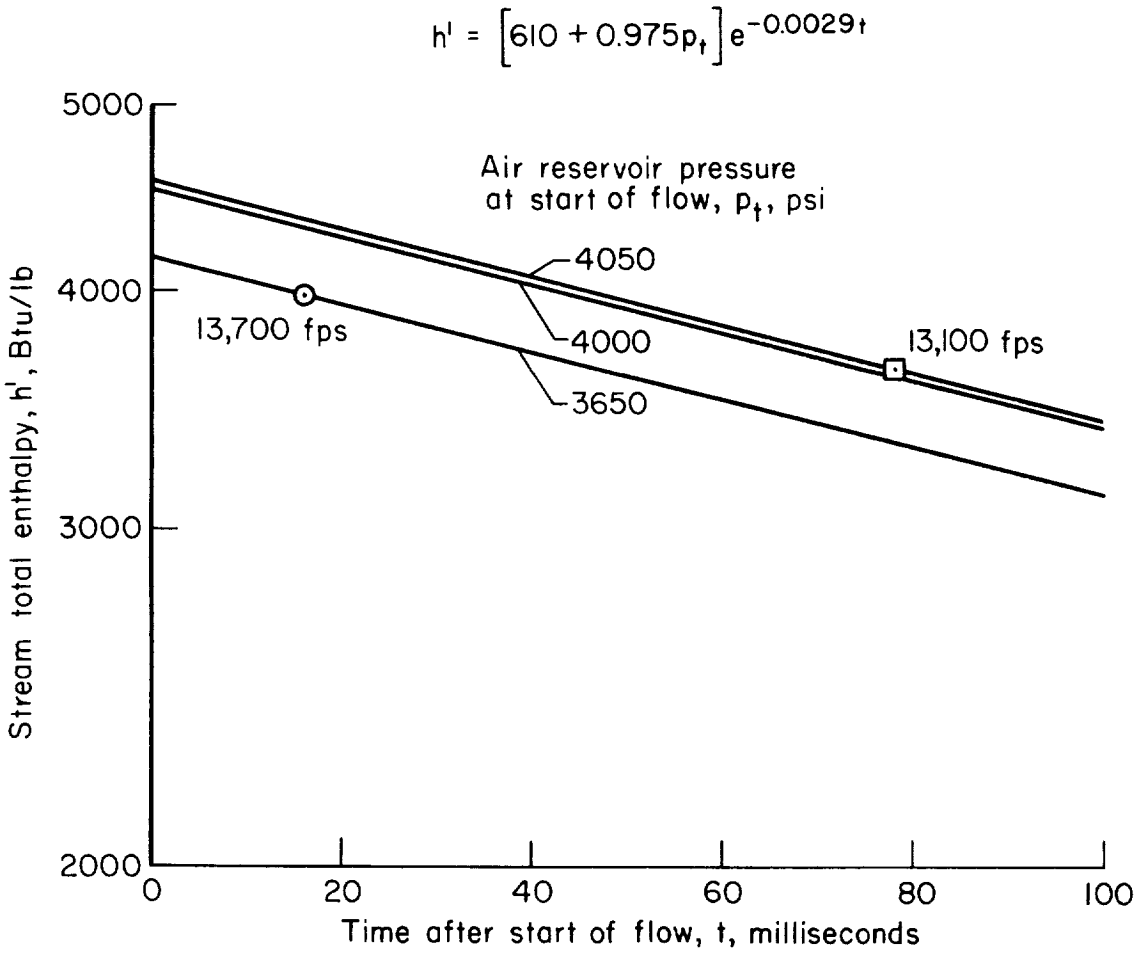

Figure 16.- Variation of stream total enthalpy with flow time.

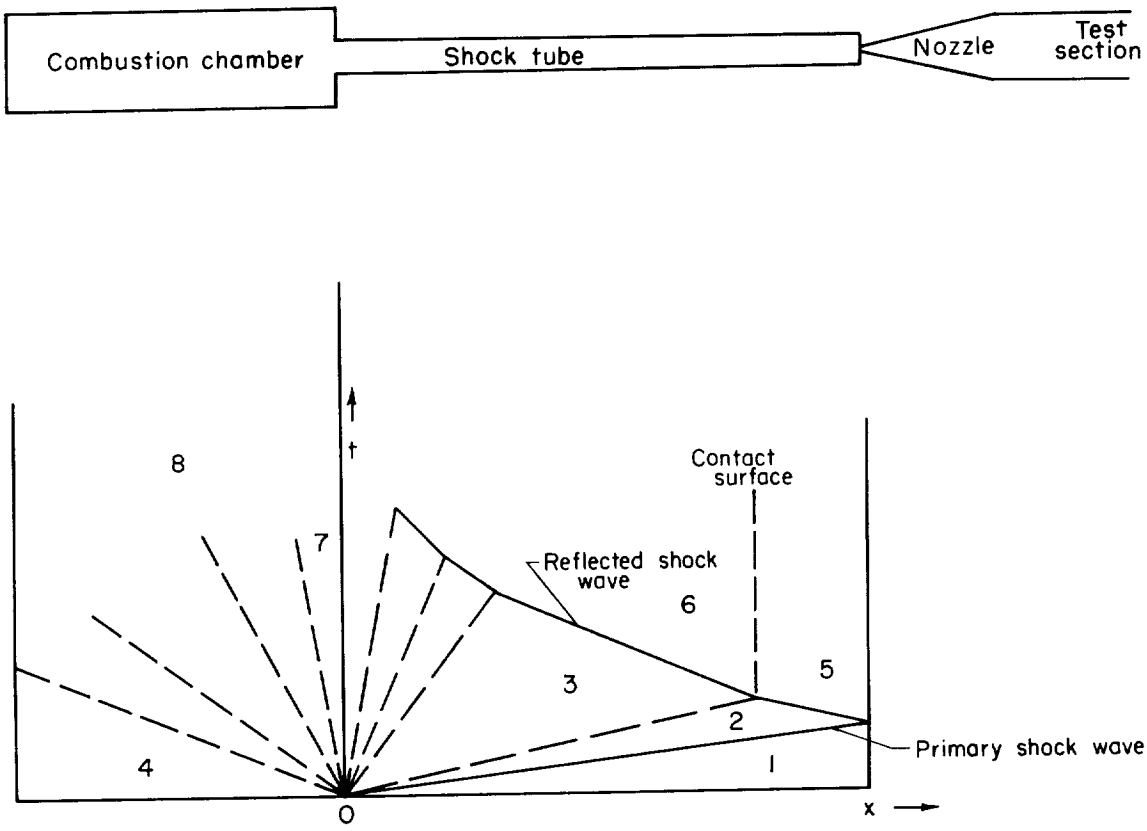

States. 1.- Air in shock tube prior to initiation of shock compression.

2.- Air in shock tube after shock compression by primary shock wave.

3.- Driver gas after expansion into shock tube.

4.- Driver gas in combustion chamber prior to initiation of shock compression.

5.- Air in shock tube (air-reservoir conditions) after shock compression by reflected shock wave ($u_5 = 0$).

6.- Driver gas in shock tube after shock compression by reflected shock wave ($u_6 = 0$).

7.- Driver gas expanding through shock-tube inlet.

8.- Driver gas in combustion chamber after completion of shock compression ($u_8 = 0$).

Figure 17.- Time-distance (or x-t) diagram of wave motion during the one-cycle shock-compression process.

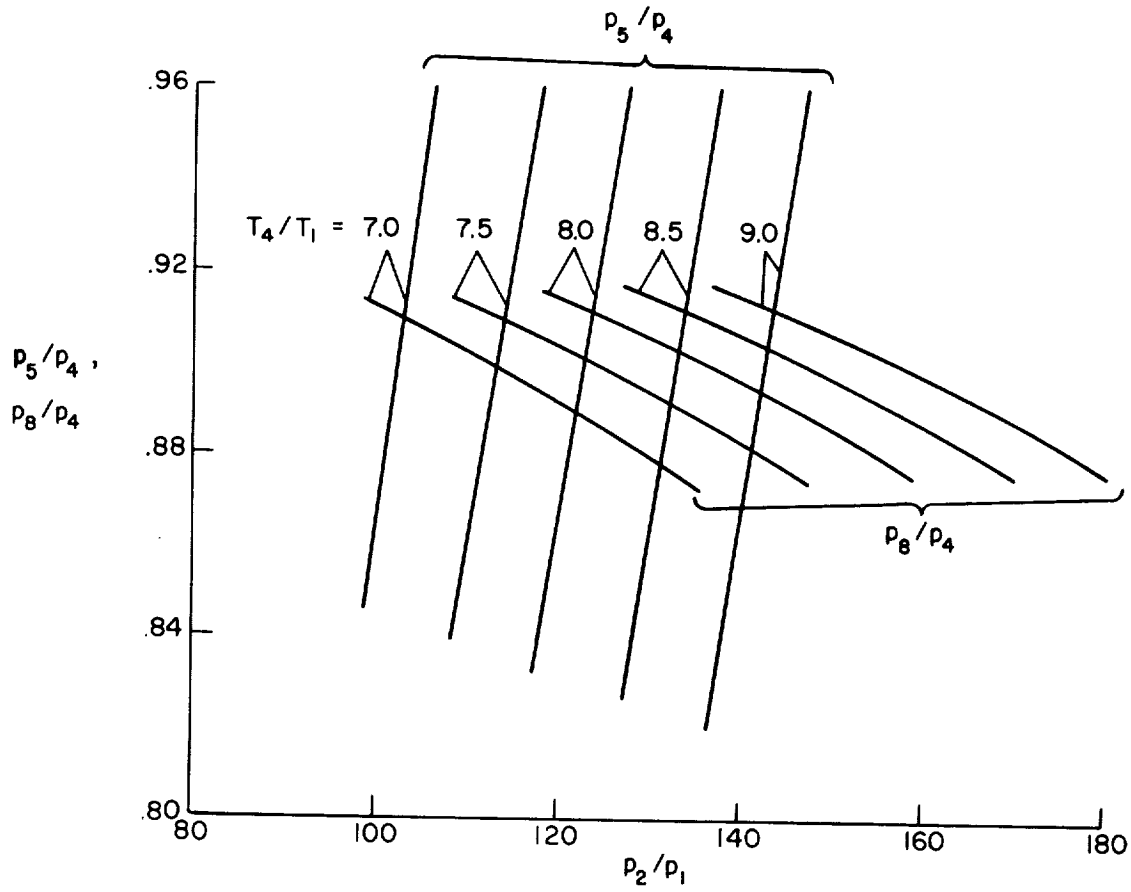

(a) Pressure ratios, p_5/p_4 and p_8/p_4, at which equilibrium pressure ($p_5 = p_6$) at the contact surface can be achieved for various values of the temperature ratio, T_4/T_1, as a function of the primary-shock-wave strength, p_2/p_1.

Figure 18.- Conditions pertinent to the achievement of one-cycle shock compression in the Ames 1-Foot Hypervelocity Shock Tunnel (p_1 = 0.1 atm., T_1 = 520° R, γ_1 = 1.4, γ_4 = 1.55, m_4 = 5.9).

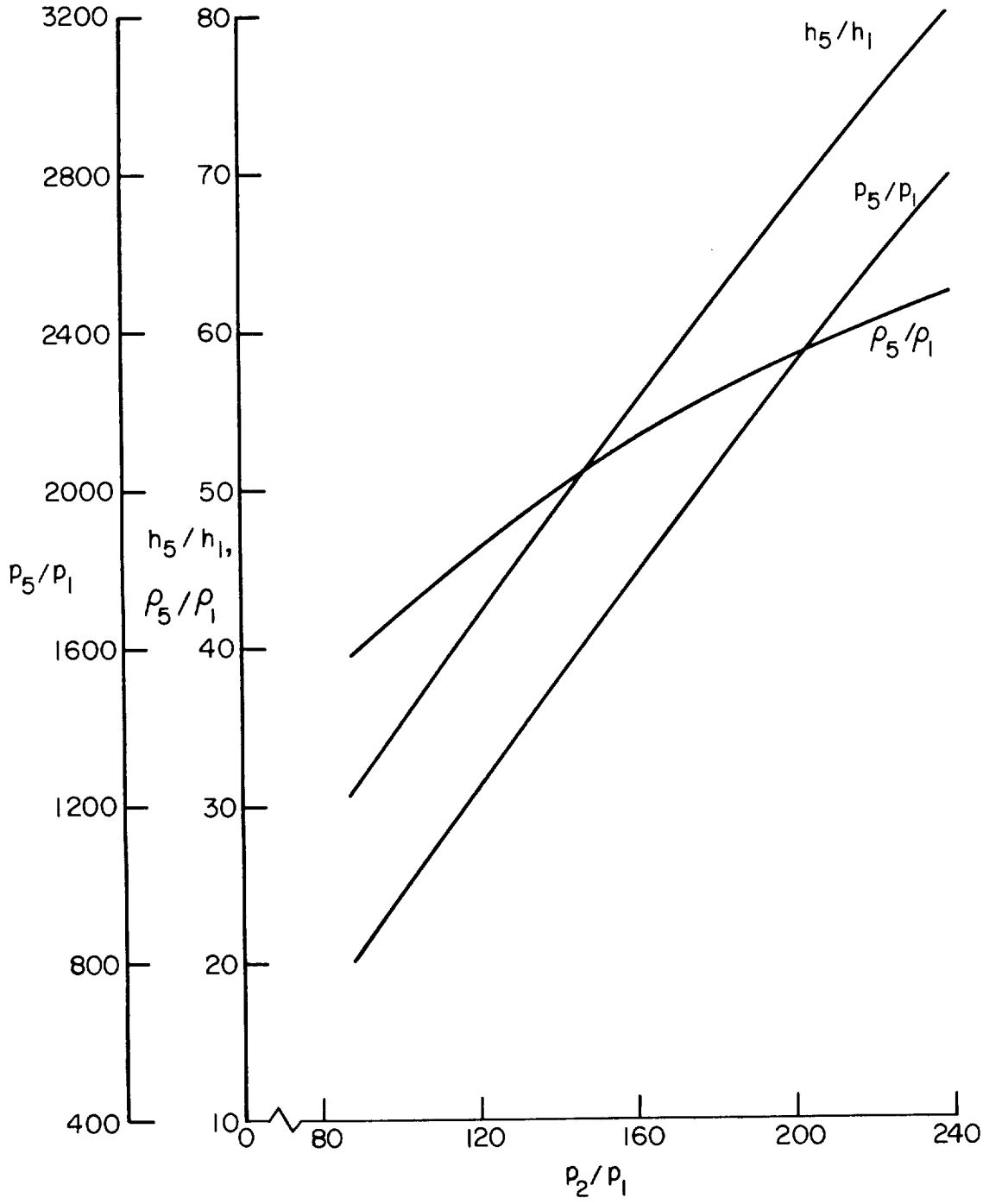

(b) Air-reservoir pressure, enthalpy, and density ratios (with respect to initial conditions) as a function of the primary-shock-wave strength, p_2/p_1.

Figure 18.- Concluded.

NASA-Langley, 1962 A-469